Lineage-specific, fast-evolving GATA-like gene regulates zygotic gene activation to promote endoderm specification and pattern formation in the Theridiidae spider

Sawa Iwasaki-Yokozawa[1], Ryota Nanjo[1,2], Yasuko Akiyama-Oda[1,3,4], Hiroki Oda[1,2,*]

[1]Laboratory of Evolutionary Cell and Developmental Biology, JT Biohistory Research Hall, Takatsuki, Osaka 569-1125, Japan

[2]Department of Biological Sciences, Graduate School of Science, Osaka University

[3]PRESTO, Japan Science and Technology Agency, Kawaguchi, Saitama 332-0012, Japan

[4]Department of Microbiology and Infection Control, Faculty of Medicine, Osaka Medical and Pharmaceutical University

*Correspondence to: Hiroki Oda (hoda@brh.co.jp)

Abstract

Background: The process of early development varies across the species-rich phylum Arthropoda. Owing to the limited research strategies for dissecting lineage-specific processes of development in arthropods, little is known about the variations in early arthropod development at molecular resolution. The Theridiidae spider, *Parasteatoda tepidariorum,* has its genome sequenced and could potentially to contribute to dissecting early embryonic processes.

Results: We present genome-wide identification of candidate genes that exhibit locally restricted expression in germ-disc forming stage embryos of *P. tepidariorum*, based on comparative transcriptomes of isolated cells from different regions of the embryo. A subsequent pilot screen by parental RNA interference identifies three genes required for body axis formation. One of them is a GATA-like gene that has been fast evolving after duplication and divergence from a canonical GATA family gene. This gene is designated *fuchi nashi* (*fuchi*) after its knockdown phenotypes, where the cell movement toward the formation of a germ disc was reversed. *fuchi* expression occurs in cells outside a forming germ disc and persists in the endoderm. Transcriptome and chromatin accessibility analyses of *fuchi* pRNAi embryos suggest that early *fuchi* activity regulates chromatin state and zygotic gene activation to promote endoderm

specification and pattern formation. We also show that there are many uncharacterized genes regulated by *fuchi*.

Conclusions: Our genome-based research using an arthropod phylogenetically distant from *Drosophila* identifies a lineage-specific, fast-evolving gene with key developmental roles in one of the earliest, genome-wide regulatory events, and allows for molecular exploration of the developmental variations in early arthropod embryos.

Background

The early processes of development and reproductive strategies of animals vary among species. In certain metazoan phyla, including Chordata and Arthropoda, a high degree of early developmental variations among species is observed, despite the identification of similar morphological traits and gene expression patterns during mid-embryogenesis in each phylum [1,2,3,4,5,6,7]. Mechanisms of animal evolution that account for varied developmental trajectories preceding the phylotypic period are poorly understood.

The species-rich phylum Arthropoda, comprising four major groups (Chelicerata, Myriapoda, Crustacea, and Hexapoda), conspicuously shows the diversification of early developmental processes without the disruption of stable embryonic traits, such as the elongating germ band and repetitive body units. Genetic mutation screens and a range of molecular and genetic techniques are feasible for the model organism *Drosophila melanogaster*, which has contributed to the identification of numerous essential genes and their interactions in body axis formation, germ layer formation, and segmentation. The *Drosophila* paradigm of genetic programs for early embryogenesis has allowed for candidate-gene approaches toward elucidating the evolution of developmental mechanisms in other insects or arthropod species. Such candidate-gene approaches, however, are biased with respect to the detection of key developmental genes; having relatively low consideration for lineage-specific, fast evolving, or orphan genes [8,9]. Conversely, comparative genomics in Arthropoda and other metazoan phyla has revealed lineage-specific genomic events, including gain/loss, expansion, or divergence of a gene or a gene family [10,11,12,13]. *bicoid, spätzle*, and *gurken* in *Drosophila*, which are key regulators in the organization of the major embryonic axes, are examples of lineage-specific or fast-evolving genes [14,15,16]. Considering these *Drosophila* cases and similar ones in different phyla [17,18,19], an

unbiased way of identifying key developmental genes is required. Therefore, several studies that used non-*Drosophila* insect species have performed genetic mutation or gene knockdown screens by assessing larval cuticle phenotypes [20,21,22,23]. However, the identification and characterization of novel genes with key functions in specific processes of early embryogenesis are hardly feasible in any non-*Drosophila* arthropods, particularly in non-insect arthropods.

In arthropods, many model species have continued to emerge, with the genome sequenced [10,24]. There have been numerous technical merits with respect to the study of early embryogenesis in one of them, the common house spider—*Parasteatoda tepidariorum*, and distinct differences from *Drosophila* have been observed in the early embryogenesis mechanism [25]. These differences include early completion of cellularization [26,27] and involvement of Hedgehog signaling in establishing the polarity of the first embryonic axis and regulating symmetry-breaking movement of the Dpp signaling center during the orthogonalization of the first and second embryonic axes [28,29,30]. In the *P. tepidariorum* experimental system, genetic regulations during early embryonic processes can be investigated using a simple gene knockdown technique, that is, parental RNA interference (pRNAi) [29]. Research using *P. tepidariorum* has been empowered by genomic and bioinformatic resources [25,31,32,33,34,35,36], thus providing the foundation for identifying key genes involved in *P. tepidariorum* development.

The egg of *P. tepidariorum* is spherical in shape (Fig. 1). As the development starts, the egg nuclei synchronously divide, approaching the surface of the egg (stage 1). Cellular organization of the embryo is established by the time the nuclei increase to 16 [26]. The initial blastoderm comprises approximately 64 cells (stage 2; 11 h AEL), showing spherical symmetry at the morphological level. This symmetry is broken at approximately 15 h AEL by the emergence of uneven cell densities toward the formation of a germ disc within a hemisphere of the egg (stage 3) (Fig. 1; Additional file 1: Movie S1), which side is designated the embryonic side. At the pole on this side, a small number of cells is apically constricted, thus forming a blastopore [25,28]. Zygotic gene activities are required for the process of germ-disc formation [37]. Although most blastoderm cells participate in the formation of the germ disc, cells derived from around the abembryonic pole do not, and remain in the non-germ-disc

region (Fig. 1; see also Additional file 1: Movie S1). The formed germ disc is sharply demarcated by the difference in cell density and comprises a single layer of more than 1,000 cuboidal epithelial cells [38]. Cells at the center of the germ disc, corresponding to the blastopore, internalize to become the central endoderm (cEND) cells and the cumulus mesenchymal (CM) cells [28,32]. The latter cell populations are clusterd and act as a dynamic source of Dpp signaling to promote the development of the dorsal side of the embryo [28,29] (Fig. 1). Cells at and near the rim of the germ disc internalize to become the peripheral endoderm (pEND) and mesoderm (pMES) cells [32]. A line of cells along the rim of the germ disc express specific genes, including a *P. tepidariorum hedgehog* homolog (*Pt-hh*), that contributes to the anterior-posterior patterning of the embryonic field [30,39,40]. The germ disc is transformed into a bilaterally symmetric germ band through orchestrated cell rearrangements, while being progressively patterned [29,38] (Fig. 1).

The formation of the sharply demarcated germ disc is an early morphogenetic event in the embryogenesis of Theridiidae and some other Araneoidea spiders [27,28, 37,41,42,43,44], but it is not a general feature of spider (Araneae) embryonic development [45,46,47]. There are many other variations in early developmental processes among spider species, including the presence/absence of a visible cumulus and various modes of gastrulation [44,48]. The spider lineage provides diverse developmental trajectories prior to reaching the embryonic traits typical of arthropods.

To explore the variation in the process of early embryonic development across the phylum Arthropoda at molecular resolution, we conducted comparative transcriptomes of cells isolated from different regions of the embryo at the germ-disc forming stage in *P. tepidariorum*. Through a pRNAi-based functional screen of differentially expressed gene candidates, we identified a lineage-specific GATA-like gene, *fuchi nashi* (*fuchi*), whose knockdown hindered the completion of germ-disc formation. We obtained genome-wide datasets that represented gene expressions and chromatin accessibilities affected by *fuch*i knockdown in early embryos. Our findings showed that *fuchi* regulates zygotic gene activation to promote endoderm specification and pattern formation in the early stage of the Theridiidae spider embryo. This study provides new molecular clues for exploring the mechanisms for diversifying early developmental trajectories in the phylum Arthropoda.

Results

Comparative transcriptome analyses of cells isolated from different regions of early *P. tepidariorum* embryos

To search for genes with locally-restricted expression in *P. tepidariorum* embryos at stage 3, we performed RNA sequencing (RNA-seq) of small cell populations (approximately 10-30 cells) isolated from central (c), intermediate (i), and peripheral (p) regions of the nascent germ disc using glass capillary needles (Fig. 2A, B). RNA-seq reads were mapped to the *P. tepidariorum* reference genome Ptep1.0 (GCA_000365465.1), and then the reads were counted against the AUGUSTUS gene models (aug3.1) [31]. The read counts were compared using edgeR [49] by setting the following three combinations: comparison I, c cells versus i/p cells; comparison II, p cells versus c/i cells; and comparison III, i cells versus c/p cells (Fig. 2C-E). Based on these comparisons, we genome-widely identified candidates of differentially expressed genes (DEGs) (Additional file 2: Tables S1-S3). Using the values of false discovery rate (FDR) and fold change (FC), the candidate DEGs were prioritized (lower FDR with $\log_2FC < -10$ [for comparisons I and II] or $\log_2FC > 10$ [for comparison III]), selecting the top 10 genes from comparison I as Group C (Fig. 2C), the top 5 genes from comparison II as Group P (Fig. 2D), and the top 5 genes from comparison III as Group CP (Fig. 2E). The top-ranked *g4238* in Group C was listed in Group CP, despite its much stronger expression in c cells than in other cells. To avoid redundancy, *g4238* was removed from Group CP. Therefore, a total of 19 genes were systematically selected as high-priority candidate genes that might exhibit locally-restricted expression in the stage-3 embryo.

To validate our gene-selection strategy, we examined the expression patterns of the 19 selected genes in stage-3 embryos using chromogenic whole-mount in situ hybridization (WISH) (Additional file 3: Fig. S1). Three of the ten Group C genes (*g4238*, *g14287*, and *g16467*) showed specific expression at the embryonic pole. Furthermore, three of the other Group C genes (*g15167*, *g5118*, *g20850*) and one of the four Group CP genes (*g26874*) showed specific expression at the embryonic pole and in a broad area on the abembryonic side. No other Group CP and Group P genes, however, showed specific detectable signals.

Additionally, similar comparative transcriptome analyses of isolated cells were applied to stage-4 and early stage-5 embryos. The resulting DEG lists (Additional file 2: Tables S4, S5) included some of the DEGs identified by the analyses of the stage-3 samples (e.g., *g4238*, and *g132*), as well as genes that had been known to show region-specific expression at the corresponding and/or later stages (eg., *Pt-lab1* [*g7954*], *Pt-BarH1* [*g8250*], *Pt-prd2* [*g18397*], and *Pt-hh* [*g4322*]).

These data suggest the effectiveness of our gene-selection strategy based on comparative transcriptome analyses of isolated cells from early *P. tepidariorum* embryos.

Pilot functional screen identifies three genes required for germ-disc formation and/or axis formation

To identify genes with key functions in the early embryonic development of *P. tepidariorum*, we screened the 19 candidate DEGs (from the stage-3 samples) using parental RNAi (pRNAi). Double-stranded RNA (dsRNA) synthesized for each gene, as well as that for a non-spider control gene *green fluorescent protein* (*gfp*), was injected into at least two adult females. Aliquots of eggs deposited by the females were placed in oil to monitor the developmental process from early stages under the stereomicroscope. Through this screening, we identified three genes whose knockdown resulted in uncommon defects associated with germ disc formation (*g26874* and *g7720*) and/or cumulus movement (*g26874*, *g7720*, and *g4238*) (Additional file 4: Table S6)[50]. To verify the RNAi specificity, we injected two or three dsRNAs prepared from non-overlapping regions of each positive gene and confirmed that the same phenotypes were produced depending on the genes (Fig. 3A; Additional file 3: Fig. S2; Additional file 5: Movie S2)[50]. In addition, we confirmed through WISH that the transcript levels of the target genes were reduced in the corresponding pRNAi embryos (Fig. 3B).

Time-lapse microscopy and cell tracking revealed that *g26874* pRNAi embryos showed normal blastoderm formation (stage 2) and subsequent initiation of cell density shift toward the formation of a germ disc, in a rather normal way, but they failed to stabilize the boundary of the forming germ disc (25 h AEL), with the cell density shift being reversed (Fig. 3A; Additional file 5: Movie S2; Additional file 6:

Movie S3). In all of such severely affected *g26874* pRNAi embryos, the initial cell thickening at the embryonic pole took place. In 64% of the *g26874* pRNAi embryos (*n* = 101 from 10 egg sacs), however, CM cell migration was faint or failed to occur. The defects in germ-disc formation were not recovered at later stages, showing no clear sign of cell movements toward the formation of a germ band. In the most severe cases of *g26874* pRNAi embryos, cells that had initially shifted toward forming a germ disc reversed their movement to spread across the embryo, followed by abrupt breakdown of the surface cell layer and extrusion of the yolk materials (Additional file 5: Movie S2)[50].

g7720 pRNAi embryos showed normal blastoderm formation followed by cell-density shift (stages 2 and 3), but its development was arrested around the end of stage 3, showing a gradually degenerating germ disc (Additional file 5: Movie S2)[50]. Although cumulus-like cell thickening was formed at the embryonic pole, it persisted there, with the overall morphology failing to develop further.

g4238 pRNAi embryos were morphologically indistinguishable from wild-type and *gfp* pRNAi (control) embryos until early stage 5. The earliest visible difference of *g4238* pRNAi embryos from normal embryos was their failure to initiate migration of the CM cells at early stage 5, followed by their disassembly and dispersal (Additional file 5: Movie S2)[50]. In many of the embryos, surface cells around the closed blastopore formed a tail-like protrusion. Despite experiencing cumulus defects, some *g4238* pRNAi embryos displayed asymmetric cell movements toward the formation of a germ band.

Molecular characterization of the three identified genes

Developmental transcript profiling in whole wild-type embryos, based on public RNA-seq datasets [36], revealed that there is little or no maternal supply of *g26874* and *g4238* transcripts and increasing levels of the zygotic transcripts prior to peaking at stage 4 (Fig. 3C). In contrast, substantial levels of *g7720* transcript appeared to be maternally supplied, with the zygotic transcript expressed at rather uniform levels through development.

Reciprocal blastp/tblastn searches using *Drosophila* and mouse reference sequence (RefSeq) protein databases at National Center for Biotechnology

Informataion (NCBI) and the *P. tepidariorum* aug3.1 transcript sequences [31] revealed that *g7720* encoded an orthologue of *Drosophila* proximal sequence element A (PSEA)-binding protein 49kD (Pbp49) and mouse small nuclear RNA-activating complex subunit 3 (Snapc3) [51], and *g4238* an orthologue of *Drosophila* Ets98B (D-ets4) and mouse SAM pointed domain-containing Ets transcription factor (Fig. 3D) [52]. *g4238* was identical to *Pt-Ets4*, as reported in a previous study [53], and consistent with our observations.

In contrast to the *g4238 and g7720* cases, reciprocal blastp/tblastn searches failed to confirm the presence of *Drosophila* and mouse orthologues for *g26874*. The best-hit *Drosophila* and mouse proteins were Pannier (Pnr), a GATA transcription factor, and GATA-4, respectively (Fig. 3D), but these proteins were significantly closer to GATA family members encoded by *g8336* and several other genes in the *P. tepidariorum* genome. Based on these results, along with those obtained from comprehensive sequence analyses described below, we concluded that *g26874* encodes a novel GATA-like gene, which we named "*fuchi nashi*" (abbreviated *fuchi*) after its knockdown phenotypes. This Japanese word means rimless.

fuchi is a lineage-specific, fast-evolving GATA-like gene

The family of GATA transcription factors are characterized by the possession of a specific DNA-binding domain, which comprises two GATA-type zinc finger (ZF) motifs (ZF1 and ZF2), typically $CX_2CX_{17}CX_2C$, and two basic regions followed by each ZF motif (BR1 and BR2) (Fig. 4A, B)[54,55]. Fuchi had this GATA-type DNA-binding domain, although its sequence was highly divergent from those of *Drosophila* Pnr and mouse GATA-4. To comprehensively understand the diversity of GATA family proteins among metazoans and the phylogenetic origin of *fuchi*, we exhaustively collected and manually aligned amino acid sequences of GATA family proteins from *P. tepidariorum*, other spider and non-spider chelicerate species as well as from other selected arthropod and non-arthropod metazoan species using publicly available bioinformatic resources (Additional file 7: Tables S7, S8). The resulting sequence alignment revealed that the metazoan GATA family members were classified under canonical and noncanonical types. The canonical type was characterized by a BR1 of 29 amino acid residues with high sequence similarity, and the noncanonical type by a

BR1 of more, or less, than 29 amino acid residues with a varying degree of sequence divergence. The canonical GATA family members included proteins encoded by five *P. tepidariorum* genes (designated Pt-GATA1 to Pt-GATA5, encoded by *g20514*, *g1834*, *g8336*, *g25261*, and *g8337*, respectively) and their counterparts from other Araneae species, as well as *Drosophila* Serpent (Srp), the only *Nematostella vectensis* GATA (Nv-GATA), two echinoderm GATAs, and mouse GATA-1 to GATA-6 (Fig. 4B-D; Additional file 7: Table S8). Phylogenetically widespread distribution of the specific sequence features suggested that the canonical GATA family members represent the ancestral state for metazoan GATA proteins.

The sequence alignment of the noncanonical GATA family members, including Fuchi, guided the identification of at least three groups specifically found within the Araneae lineage, based on gap insertion patterns, cysteine residue spacing, and sequence signatures (Fig. 4C, D; Additional file 7: Table S8). These three groups were designated as GATA-like 1 to 3 (GATAL1, GATAL2, and GATAL3). GATAL1, which included a *P. tepidariorum* protein encoded by *g26871* (Pt-GATAL1), was relatively close to the canonical GATA family members at the sequence level, but they had a BR1 of 34 amino acid residues. GATAL2, which included Fuchi and another *P. tepidariorum* protein encoded by *g26875* (designated Pt-GATAL2b), was specifically identified by a signature sequence QCV(K/R)CG at the N-terminal end of ZF1, varied cysteine residue spacing in ZF1 ($CX_2CX_{17\text{-}20}CX_2C$), and a highly varied number (23-44) of amino acid residues in BR1. GATAL3, which was only found in spiders of RTA clade, was specifically identified by conserved unique sequences and cysteine residue spacing ($CX_2CX_{18}CX_2C$) in ZF1. The signature sequence unique to GATAL2, QCV(K/R)CG, corresponded to ECVNCG, conserved in most canonical GATA family members (including Pt-GATA1 to 4) and GATAL1, to QC(A/V)(M/V)CG, conserved in Pt-GATA5 and its counterparts, and to ECANCG, conserved in GATAL3.

To investigate the phylogenetic relationship between canonical and noncanonical GATA family proteins, we performed maximum likelihood (ML) analysis using unambiguously aligned 75 amino acid sites from a total of 118 proteins with both ZF1 and ZF2 representing the typical cysteine residue spacing ($CX_2CX_{17}CX_2C$) (Fig. 4E, F; Additional file 7: Table S8). Results showed Araneae-specific expansions of GATA protein family members, through gene duplication and divergence. ML tree

topology supported the orthology of each of the GATA5, GATAL1, and GATAL2 groups. Furthermore, branch lengths indicated that the sequences of the GATAL2 proteins had been evolving much faster than those of the canonical GATA family and GATAL1 proteins (Fig 4F). Owing to their atypical cysteine residue spacing in ZF1 ($CX_2CX_{18\text{-}20}CX_2C$), Fuchi and other Araneoidea GATAL2 proteins could not be included in the ML analysis (Fig. 4C; Additional file 7: Table S8). Importantly, GATAL2 proteins with the typical ZF1 ($CX_2CX_{17}CX_2C$), which were used in the ML analysis, were present in a broader phylogenetic range (including Leptonetidae, Eresidae, and RTA clade) (Fig. 4C, E, F; Supplementary Table 4). This observation suggested that variously divergent sequences in ZF1 of the Araneoidea GATAL2 proteins, except the specific signature sequence, were likely due to rapid sequence evolution from the GATAL2 ancestral state.

Unlike the other two of the three genes judged as positive in the functional screen, *fuchi* was characterized as a lineage-specific gene. We therefore decided to focus our later analyses on this gene.

fuchi is expressed in endoderm cells originating from both sides of the early embryo

Among the eight GATA family genes in *P. tepidariorum*, *fuchi* was the only gene which was transcribed at substantial levels during the germ-disc forming stage (stage 3) (Fig. 3C; Additional file 3: Fig. S3). We investigated the expression of *fuchi* transcript in early embryos at cellular resolution, using conventional WISH and the combination of FISH with antibody staining for β-catenin, which serves as a marker for regions of cell-cell contact (Fig. 5). Owing to technical limitations in the fixation of stage-1 embryos, the earliest stage of development examined was stage 2, the blastoderm stage (13 h AEL), when there is no morphological sign of asymmetry reflecting the future embryonic axes. At this stage, localized signals for *fuchi* expression were detected on one side of the embryo (Fig. 5A, A', B, B') but could not be related with the axis that would emerge a little later (15 h AEL).

At early stage 3 (15 h AEL), the embryo begins to display morphological asymmetries, with an emerging embryonic-abembryonic (Em-Ab) axis (Fig. 1). At this stage and later, the *fuchi* transcript was detected in a small number of cells condensed

at the embryonic pole (Fig. 5I, I', I") and in a larger number of cells showing a progressively wider distribution on the abembryonic side of the embryo (Fig. 5J, J', J"). Using a flat-preparation of a representative early stage 3 (15 h AEL) embryo stained for *fuchi* transcript, the number of *fuchi*-expressing cells was counted. There were 8 and 20 *fuchi*-expressing cells around the embryonic pole and on the abembryonic side, respectively, among a total of approximately 300 cells (Additional file 3: Fig. S4). Notably, signals for *fuchi* transcript in the nuclei were, in many cases, observed as paired dots (Fig. 5I', J'), indicating that the zygotic transcription was already active at early stage 3. In the equatorial area of stage 3 embryos (15 and 21 h AEL), there was a transition from cells expressing *fuchi* transcript, on the abembryonic side, to those not expressing it, on the embryonic side (Fig. 5J, J', J", K, K', K"). In the embryo at 21 h AEL, the *fuchi*-expressing cells had larger apical surfaces than the *fuchi*-negative cells (Fig. 5K').

In embryos at stage 4 (25 and 27 h AEL), most *fuchi*-expressing cells on the abembryonic side had further enlarged surfaces with less tensed lines of cell-cell contact, which contrasted with a tightly packed organization of *fuchi*-negative cells constituting the nascent germ disc on the embryonic side (Fig. 5D, L, M, M', M"). A few *fuchi*-expressing cells, however, were identified as part of the germ disc at its border (Fig. 5M', M"). At the blastopore, cEND cells and CM cells are internalized (Fig. 1). *fuchi* expression was observed in all these internalizing and internalized cells (Fig. 5L, L', L").

In embryos at stage 5 (32 and 38 h AEL), all cells internalized through the blastopore continued to express *fuchi* (Fig. 5E, E', F, F', N, N1', N1", O, O1"). Peripheral populations of *fuchi*-expressing cells appeared to be internalized a little later than the central populations. At early stage 5 (32 h AEL) *fuchi*-expressing cells on the embryo surface were found not only in the non-germ disc region but also at the rim of the germ disc (Fig. 5N, N2', N2"). At late stage 5 (38 h AEL), there were *fuchi*-expressing cells that were internalized/internalizing from or through the rim of the germ disc (Fig. 5F, F', O, O2', O2"). Using a DNA stain probe, SPY555-DNA, we tracked some cell nuclei in the germ-disc/non-germ-disc transition area from early stage 5 to stage 8 in a live embryo (Additional file 4: Movie S4), which directly visualized two phases of cell internalization. Phase 1 of cell internalization occurred from mid to late

stage 5, where cells that were not part of the germ disc were approaching the rim of the germ disc and then internalizing to below the surface cell layer of the germ disc. These were most likely to be *fuchi*-expressing cells. Phase 2 of cell internalization occurred subsequently, where cells at the rim of the germ disc were internalizing. Double staining for *fuchi* and *Pt-hh* transcripts revealed that certain cells at and near the rim of the germ disc at early stage 5 expressed both *fuchi* and *Pt-hh* (Fig. 5P, P'). Upon internalization, however, *fuchi*-expressing cells were exclusively *Pt-hh*-negative (Fig. 5Q, Q').

To determine whether *fuchi*-expressing cells internalized from the peripheral side of the germ disc are endoderm or mesoderm, double staining of late stage 5 and stage 6 embryos for *fuchi* and *Pt-fkh* (a marker for pMES plus pEND; [56]) or *003_J01* (a marker for pMES)[57] was performed. The use of *003_J01* enabled us to identify pMES cells prior to internalization, which was not the case with *Pt-twi*, another pMES marker [32,56,58]. Observations indicated that all internalized, *fuchi*-expressing cells were *Pt-fkh*-positive and most of them were *003_J01*-negative (Additional file 3: Fig. S5). It was also indicated that *003_J01*-positive cells appeared to be internalized later than *fuchi*-expressing cells, which presumably corresponded to Phase 2 of cell internalization. *fuchi* expression in embryos at stages 6 and 7 never showed a spatially periodic pattern along the emerging body axis (Fig. 5G, G', H, H'), contrasting with mesoderm marker expression [58]. Taken together, these data suggested that *fuchi* is expressed in endoderm cells originating from both sides of the early embryo. In addition, *fuchi* expression occurred in association with extraembryonic differentiation (Fig. 5G, G', H, H'). This *fuchi* expression was already initiated in the germ disc at late stage 5 (Fig. 5O, O1").

***fuchi* knockdown prevents the demarcation of a forming germ disc**

To investigate the defects following *fuchi* knockdown, we analyzed the expression of *Pt-hh*, *Pt-fkh*, and *fuchi* transcripts in wild-type and *fuchi* pRNAi embryos at stage 4 and early stage 5 at cellular resolution. In normal germ-disc development, a line of cells expressing *Pt-hh* and *Pt-fkh* was organized to demarcate the boundary of the forming germ disc during stage 4 and early stage 5 (Fig. 6A, A', C, C', E, E', G, G'). In the recognizable germ-disc/non-germ-disc transition area of *fuchi* pRNAi embryos at stage

4, the initial *Pt-hh* expression was strongly suppressed, while *Pt-fkh* expression was detectably initiated in certain cells with *fuchi*-positive nuclei and their neighboring cells (Fig. 6B, B', D, D'). At early stage 5, faint *Pt-hh* and *Pt-fkh* expression were detected in small numbers of cells, but they did not contribute to shaping the germ disc (Fig. 6F, F', H, H'). In *fuchi* pRNAi embryos at a later stage (late stage 5), there was no clear separation between cell populations on the embryonic and abembryonic sides, with cell internalizations being highly limited (Fig. 6I, I1', I1", I2', I2"). The only cells situated below the surface layer were cells at or near the embryonic pole (Fig. 6I1', I1"), which were associated with β-catenin concentrations marking the CM cell cluster. These observations suggested that *fuchi* knockdown prevented the demarcation of a forming germ disc and interrupted the formation of the germ layers.

fuchi is required for zygotic activation of endodermal and patterning genes

To explore the role of *fuchi* in regulating early *P. tepidariorum* development, we conducted comparative transcriptome analyses of *fuchi* pRNAi versus untreated embryos at stages 2, 3, and early stage 5 using RNA-seq. These analyses identified 6, 139, and 785 DEGs for stages 2, 3 and early stage 5, respectively (FDR<0.01; Fig. 7A, B; Additional file 9: Tables S9-S11). The experiments were validated by detecting lowered levels of *fuchi* transcript and unaffected levels of the α-catenin (*catA*) transcript in the *fuchi* pRNAi samples (Fig. 7C). Except for the *fuchi* gene itself, there was no overlap between the stage-2 and stage-3 DEGs but there was an overlap of 93 genes between the stage-3 and early stage-5 DEGs (Fig. 7B; Additional file 9: Tables S9-S11). According to NCBI's gene annotation, 26 of the 93 DEGs encoded uncharacterized proteins. Transcripts for the stage-2 DEGs appeared to be maternally supplied (Additional file 3: Fig. S6), which contrasted with those for highly ranked genes from the stage-3 and early stage-5 DEGs lists (sorted by FDR value). They tended to show a sharp increase in the transcript level during stages 2 to 4, with no or little transcript supply from the mother (Fig. 7C, D). All the top 20 genes from the stage-3 DEG list were included in the stage-5 DEG list (Fig. 7D; Additional file 9: Table S10). Blastx searches against mouse and *Drosophila* RefSeq protein databases resulted in no hits for seven of the top 10 DEGs (E-value < 1e-5) (Fig. 7C). Transcripts from 8 of the top 10 DEGs (*g1125*, *g2114*, *g20850*, *g17950*, *g12453*, *g27539*, *g486*, and *g26914*)

were detected in all or part of the internalized endoderm at late stage 5, and those from 3 of the 8 genes (*g17950*, *g12453*, *g20850*) were detected in cells on the abembryonic side at stage 3 (Additional file 3: Fig. S7). Notably, the *g20850* was identified as one of the Group C genes in the initial comparative transcriptome analysis of isolated cells (Fig. 2C; Additional file 3: Fig. S1).

The stage-3 *fuchi* pRNAi DEG list also included several genes previously characterized as key regulators of embryonic patterning in *P. tepidariorum*, such as *Pt-hh* (*g4322*)[30], *Pt-sog* (*g23966*)[29], and *Pt-Delta* (*g25248*)[32] (Additional file 3: Fig. S8; Additional file 9: Table S10). Despite the effects of *fuchi* knockdown on the expression of these patterning genes, certain patterning events involving *Pt-msx1* and *Pt-Delta* expression were initiated around the blastopore in *fuchi* pRNAi embryos (Additional file 3: Fig. S8). *fuchi* knockdown led to a lack of circular patterns of *Pt-hh* and *Pt-otd* expression associated with anterior patterning, but its effects on the *Pt-hh* and *Pt-otd* expression levels in whole embryos at early stage 5 were limited.

Taken together, these results suggested that *fuchi* is required for the zygotic activation of a set of endodermal genes and of some patterning genes at stage 3 or shortly before. In addition, *Pt-GATA4* (*g25261*), the likely counterpart of *Drosophila srp* (Feitosa et al., 2017), and *Pt-GATA5* (*g8337*) were included in the stage-5 *fuchi* pRNAi DEG list but not in the stage-3 one (Additional file 9: Tables S9, S10).

***fuchi* is involved in regulating chromatin accessibility in specific genomic regions in early embryos**

Certain GATA family members act as pioneer transcription factors that can influence chromatin structure [59]. Therefore, we considered the possibility that *fuchi* controls the transcription of downstream genes through chromatin structure regulation. To investigate this possibility, we conducted assay for transposase-accessible chromatin using sequencing (ATAC-seq) of wild-type (untreated), *fuchi* pRNAi, and *Pt-hh* pRNAi embryos at stage 3 (18h AEL), obtaining genome-wide datasets on chromatin accessibility. Read counts in ATAC-seq peaks were subjected to comparative analyses, and 317 genomic regions that were differentially accessible between the *fuchi* pRNAi and untreated samples but only 3 between the *Pt-hh* pRNAi and untreated samples were identified (Fig. 8A; Additional file 10; Tables S12, S13; Additional file 11; Tables S14,

S15; FDR<0.05). This indicated that the *Pt-hh* pRNAi samples served as a negative control for assessing the impact of *fuchi* knockdown. The two comparisons revealed only one shared genomic region (Fig. 8A; Additional file 10; Table S13; Additional file 11; Table S15), which potentially reflected a nonspecific effect stemming from pRNAi treatment. Therefore, 316 genomic regions where chromatin accessibility was significantly affected following *fuchi* knockdown in stage-3 embryos were identified (Fig. 8B).

Most of these regions (276/316, 93%) showed suppressed accessibility upon *fuchi* knockdown (Fig. 8A, B), and 30 of them were found to be located closer to (or within) genes included in the *fuchi* pRNAi DEG lists (for stage-3 and/or early stage-5) than to any other annotated genes (Fig. 8B; Additional file 10: Table S13). Moreover, motif discovery search revealed that motif sequences RNWGATAAGAVW, similar to typical GATA-binding motif sequences, were significantly enriched among the sequences of the *fuchi*-dependent chromatin accessibility peaks (Fig. 8C). *fuchi*-dependent chromatin accessibility peaks containing these motif sequences were actually present within or close to some of the genes identified by the comparative transcriptome analyses of *fuchi* pRNAi versus untreated embryos (Fig. 8B).

Notable examples of such genes were the top-ranked gene from the stage-3 *fuchi* pRNAi DEG list (*g1125*), the key patterning gene *Pt-hh* (*g4322*), and the canonical GATA family member *Pt-GATA5* (*g8337*) (Fig. 9A, B, C). *g1125* was predicted to encode an uncharacterized product containing two potential transmembrane domains (XP_015915605.1; Fig. 9D). Genes encoding homologous proteins to this product were detected in the genomes of at least three other Araneoidea species, *Araneus ventricosus* (GBO06802.1), *Argiope bruennichi* (KAF8764632.1), and *Oedothorax gibbosus* (KAG8179838.1)(Fig. 9D), but any non-Araneoidea protein sequences that showed similarity to these products (E-value < 1) were not found in the NCBI non-redundant protein sequences collection (March 7, 2022). *Pt-GATA5* transcript, like *fuchi*, was observed in cEND, CM, and pEND cells at stage 5 and widely distributed endoderm cells at stage 7 (Fig. 9E, F). Altogether, these results suggested that *fuchi* is required for establishing “open” states of chromatin structure in specific genomic regions, some of which are associated with endodermal and patterning genes expressed in the early stages.

480

481 **Detection of consistent endodermal gene expression based on single-nucleus and**
482 **single-cell RNA-seq datasets**

483 In a recent separate study, we performed single-nucleus and single-cell RNA-seq
484 analysis of late stage 5 embryos in *P. tepidariorum* [60]. In this study, clearly isolated
485 endodermal cell clusters, which were marked by a known early endoderm marker
486 012_A08 [56], were identified (Additional file3: Fig. S9). Strong *fuchi* expression was
487 detected in these clusters, with weaker levels of *fuchi* expression being additionally
488 detected in mesodermal (marked by *Pt-twi*)[58] and dorsal germ-disc (marked by *Pt-*
489 *GATA1*)[60] cell populations. At the same time, the endoderm-specific expression of
490 *Pt-GATA4* and *Pt-GATA5* was confirmed. In contrast to *fuchi*, and the two canonical
491 GATA genes, *Pt-hh* expression was missing or largely reduced in the endodermal cell
492 populations at late stage 5. These data were consistent with the staining data shown in
493 Fig. 5 and Fig. S5 (Additional file 3). The single-nucleus and single-cell RNA-seq
494 datasets further confirmed that most of the high-ranking genes from stage-3 *fuchi*
495 pRNAi DEG list showed endoderm-specific expression at late stage 5 (Additional file
496 3: Fig. S10).

497

498 **Discussion**

499 We conducted genome-based research using the spider *P. tepidariorum* to explore the
500 variations in the mechanisms of early embryonic development in the phylum
501 Arthropoda. A key initial attempt in this study was to analyze transcriptomes of cells
502 isolated from different regions of the early spider embryo. This allowed for the
503 genome-wide identification of candidate genes whose expression might be locally
504 restricted along the emerging first embryonic axis, without relying on knowledge from
505 other organisms. Although similar approaches to identifying localized transcripts in
506 early animal embryos have been reported in non-arthropod animals [17,61,62], early
507 arthropod embryos are rarely studied in such a way.

508 A benefit of using *P. tepidariorum* is the applicability of a simple gene-
509 knockdown technique, that is, pRNAi. This allowed us to carry out a functional screen
510 of some of the listed genes. Gene-specific embryonic phenotypes were obtained using
511 3 of the 19 genes tested (15%). Compared with similar screening efforts we previously

made following sequence-based gene selection, this small proportion is not surprising [30]. Although similar RNAi-based gene knockdown is available in certain arthropods, such as *Tribolium castaneum*, it is important to note that the *P. tepidariorum* system allows for the easy monitoring of early embryonic developmental processes, even following pRNAi treatment. Time-lapse recording of the phenotypes from early stages gave sharable, rich, objective information on gene functions and the timing of their actions. Early defects often lead to reduced characteristic morphologies at later stages. Exclusion of common spontaneous defects is required for effective functional screening. Direct detection of the earliest developmental defects following knockdown treatments in the initial screening could simplify the structuring of our interests. Despite the small scale of the functional screen we conducted, incomparable with the large-scale, unbiased RNAi screen in *Tribolium* [23], our results may encourage additional gene-function screens in *P. tepidariorum*.

Unexpectedly, our pRNAi screen found that the cell movement toward the formation of a germ disc was reversed following the knockdown of a GATA-like transcription factor gene, which we named *fuchi nashi* (*fuchi*). This phenotype suggests the presence of a shape-stabilizing phase in the germ-disc development, which likely corresponds to stage 4, during which a line of cells along the border is organized to gain specific gene expressions. *fuchi* expression, however, is initiated much earlier than this stage, in cells outside a forming germ disc, and later continues in all internalizing and internalized endoderm cells. Our comparative transcriptome and chromatin accessibility analyses of *fuchi* pRNAi versus untreated embryos suggested that early *fuchi* activities have broad impacts on zygotic gene activation around stage 3. Lack of the *fuchi* activities appeared to hinder the specification of endoderm fates. The abnormal reversed cell movements in *fuchi* pRNAi embryos could be, at least in part, explained if we assume that the different cell types being specified exhibit different mechanical properties. The earliest morphological defects of *fuchi* pRNAi embryos possibly result from a failure to establish the differences in adhesion tension between cell populations.

We showed that early *fuchi* activities influence the expression of some of the key signaling genes involved in embryonic development and pattern formation. These include *Pt-hh*, *Pt-Delta*, and *Pt-sog*. *Pt-hh* and *Pt-Delta*, down-regulated in response to

544 *fuchi* knockdown at stage 3, are known to show expression patterns similar to *fuchi* in
545 early embryos (stages 3 and 4) [30,32], and *Pt-sog*, up-regulated oppositely, to be
546 expressed in broad domains of the stage-5 germ disc [29]. Notably, early *Pt-hh*
547 expression initiated from the abembryonic side contributes to the formation of the
548 global polarity in the germ disc and subsequent anterior patterning. In *fuchi* pRNAi
549 embryos, however, no patterning events that should occur from the abembryonic side
550 of the egg were identified. These findings suggest that early *fuchi* activities specify
551 endoderm fates and promote pattern formation in a wide area of the embryo, at the
552 same time. Similar GATA factor-mediated regulation of *hh* expression has been
553 documented in several mammalian and *Drosophila* developmental events [63,64,65].
554 The family of GATA transcription factors is known to regulate cell fate
555 specification and cell differentiation during various developmental processes in a wide
556 range of animals [67]. Our functional and phylogenetic characterization of *fuchi*
557 provide the opportunity to reconsider the relationship between the evolution of GATA
558 family members and their developmental roles. We defined "canonical" members of
559 the GATA family, as they have perfectly alignable, close sequences to each other
560 throughout the double zinc-finger DNA-binding domain regardless of the phylogenetic
561 distance of the species. The canonical members include all six GATA paralogs in
562 vertebrates, GATA-1 to GATA-6, the only *Nematostella* GATA, *Drosophila* Serpent
563 (Srp), and five *P. tepidariorum* GATA paralogs, Pt-GATA1 to Pt-GATA5. The
564 vertebrate GATAs are phylogenetically classified into two subgroups: GATA-1/2/3
565 and GATA-4/5/6, while Srp is closer to GATA-4/5/6 [55,68]. *srp* functions for
566 endoderm specification in early *Drosophila* embryos [69], and vertebrate GATA-4/5/6
567 genes have developmental roles in endodermal cell lineages [70,71,72,73]. Notably, in
568 mammals, GATA-6, in cooperation with GATA-4, is essential in the specification of
569 the primitive and definitive endoderm, through chromatin accessibility regulation
570 [74,75]. Based on these lines of evidence, the idea that the roles of GATA-4/5/6 genes
571 in endoderm specification and development are conserved across bilaterians has been
572 widely accepted. Consistent with this idea, single-cell and single-nucleus
573 transcriptomes indicated that the likely *srp* ortholog *Pt-GATA4* (*Pt-srp*) appears to be
574 expressed in an endoderm-specific manner at least at late stage 5 of *P. tepidariorum*
575 development (Additional file 3: Fig. S9), although a previous report mentioned that

"*Pt-srp* expression starts at stage 8 in the presumptive extraembryonic cells." [76] Evidently, developmental transcriptomes gave a quantitative indication that there is little *Pt-GATA4* expression at stage 4 and earlier but substantial expression at late stage 5 and later (Additional file 3: Fig. S3). We suggested that instead of *Pt-GATA4*, *fuchi* and *Pt-GATA5* are key GATA family genes contributing to endoderm specification and development in the earlier stages of *P. tepidariorum* development. Although *Pt-GATA5* is a canonical member of the GATA family, it appears to have no orthologous counterpart outside the Araneae. Fuchi is not a canonical GATA factor, having a highly diverged sequence with retaining the dual zinc fingers. *fuchi* appears to act on *Pt-GATA5*, possibly through chromatin accessibility regulation. The *fuchi*-dependent ATAC-seq peak detected in the *Pt-GATA5* locus is located in an intron between exons encoding the two zinc fingers. Sequential regulation of multiple GATA factors in early endoderm specification and the subsequent differentiation process is a shared feature among distantly related bilaterians, including mouse, *C. elegans* and *Drosophila* [75,77,78]. However, the genetic components responsible for this regulation exhibit no orthologous relationships between the species, even within the Arthropoda, suggesting independent modifications of the GATA-mediated regulatory system for endoderm specification and development in the respective animal lineages.

fuchi and its orthologs (GATAL2) were found in sub lineages of the Araneae, including many Araneomorphae taxa but not non-Araneomorphae. These GATA-like genes, regardless of the cysteine spacing patterns in ZF1, have been rapidly evolving their sequences compared to most other GATA and GATA-like genes. Despite this divergence trend, we could define the likely orthologous GATAL2 group using the conservative signature sequence QCV(K/R)CG. Because the amino acid residues homologous to this sequence are involved in binding to specific cofactors, such as the vertebrate Friend of GATA (FOG) and *Drosophila* U-shaped (Ush), in canonical GATA factors [79,80,81], Fuchi possibly binds to a unique cofactor via this sequence. In relation with GATA cofactors, one of two *P. tepidariorum* homologs of *Drosophila* Ush (*g14866*; the other homolog is *g16893*) was included in both the gene lists obtained from the comparative RNA-seq and ATAC-seq analyses using stage-3 *fuchi* pRNAi embryos (Fig. 8; Additional file 9: Table S10; Additional file 10: Table S13). Certain GATA cofactors are known to exert an inhibitory effect to complicate the GATA

608 factor-mediated transcriptional regulation [63,64,82]. Such an inhibitory effect of a
609 GATA cofactor potentially accounts for the transient *Pt-hh* expression in the early
610 abembryonic cell population. High degrees of sequence divergence in the DNA-
611 binding domain of Fuchi and other GATAL2 proteins may be an indication of evolving
612 interactions with cofactors and DNA-binding sites. Previous studies have suggested
613 that N-terminal zinc fingers (ZF1) influence selectivity of DNA-binding sequences
614 [81,83]. Alternatively, the sequence divergences might have simply resulted from
615 reducing degrees of functional constrains. Future studies will focus on testing these
616 possibilities.

617 The phylogenetic origin of the *fuchi* activity in early endoderm specification
618 and those of the regulatory connection between *fuchi* and *Pt-GATA5*, is an intriguing
619 issue that provides molecular clues regarding the diversification mechanism of the
620 process of early embryonic development. The formation of a sharply demarcated germ
621 disc is not a common feature of early spider development. In Theridiidae spider
622 embryos, the formation of the germ disc involves an appearance of two distinct
623 endoderm or endoderm-like cell populations derived from both polar regions of the
624 early embryo, and the formed sharp boundary of the germ disc serves as sites of
625 endoderm and mesoderm cell internalization, as well as sites of sending patterning
626 signals [30,32,41,44]. These developmental strategies have potential merits of gaining
627 parallel processes, which may allow for a more rapid development. In the embryos of
628 many other spider species, including three distinct examples from outside the
629 Araneoidea, *Cupiennius salei* [45], *Pholcus phalangioides* [46], and *Hasarius adansoni*
630 [84], cell movements causing the germ layers only occur from one of the polar regions,
631 which corresponds to the embryonic pole or the center of the germ disc in the *P.*
632 *tepidariorum* embryo. The technical term "germ disc" results in potential confusions in
633 documenting the Theridiidae embryonic development. This term is, in certain cases,
634 used to indicate the multicell-layered region of the embryo that results from germ layer
635 formation in spiders and other arthropods [85]. The initial germ disc in Theridiidae
636 embryos, however, is a form of a single epithelial cell layer that precedes the formation
637 of the germ layers [26,27,37]. *fuchi* serves as a molecular marker for the cells outside
638 the forming germ disc. *fuchi* homologs may aid in identifying the existence of an
639 evolutionarily conserved abembryonic cell type in other spider species. Complicatedly,

the *P. tepidariorum* genome has a paralog of *fuchi* that was presumably generated by recent tandem gene duplication. No corresponding paralog was detected in other Theridiidae and non-Theridiidae spiders. The *fuchi* paralog, *Pt-GATAL2b*, shows little expression at least during the early and mid embryogenesis of *P. tepidariorum*. Studies on the expression and function of *fuchi*/*Pt-GATAL2b* and *Pt-GATA5* orthologs in the early embryos of other spider species enable us to further address the problems on the early developmental variations among the Araneae lineages.

This study has produced genome-wide datasets related to molecular and genetic regulation of early embryonic development in *P. tepidariorum*, which can be integrated with single-nucleus and single-cell RNA-seq datasets established in another study [60]. These data resources, as well as the research strategies presented, will facilitate our efforts to dissect the early developmental processes at molecular resolution and establish an independent paradigm of genetic programs for early arthropod development. Importantly, many of the genes revealed in this study encode proteins not yet characterized, thus underscoring the importance of taking genome-based approaches to studying the evolution of animal development.

Conclusions

Using a Theridiidae spider empowered by genome sequencing, we combined comparative transcriptomes of isolated cells from different regions of early embryos and a pRNAi-based functional screen of genes. This research strategy allowed us to identify a lineage-specific, fast-evolving GATA-like gene, *fuchi*, that is essential for early embryonic development in the spider. *fuchi* is expressed in future endodermal cell poupulations in the early embryo. Further genome-wide analyses suggest that *fuchi* regulates chromatin state and zygotic gene activation to promote endoderm specification and pattern formation. The presented datasets have rich information about the molecular regulation of early embryonic development in the Theridiidae spider. The presence of many uncharacterized genes under the control of *fuchi* has been revealed. Our genome-based research using a chelicerate arthropod phylogentically distant from *Drosophila* provides the foundation for molecular and genetic exploration of the variations in early development across Arthropoda.

672 **Materials and Methods**

673 **Spiders**

674 Laboratory stocks of *P. tepidariorum* were maintained at 25 ℃ in 16 h light/8 h dark
675 cycles. Developmental stages of the embryo were determined according to the previous
676 descriptions [28,58]. To determine the precise time of egg laying, female behaviors
677 were recorded every 5 min using a trail camera. The animal experimentation described
678 was approved by the institutional committee for animal care and use (No. 2020-1) and
679 conducted according to JT Biohistory Research Hall Regulation on Animal
680 Experimentation.

681

682 **Cell isolation**

683 Embryos at stage 3 were dechorionated with 50% commercial bleach for 1 min and
684 rinsed several times with distilled water. After removing water, the embryos were
685 placed on a glass slide with double-sticky tape and immediately covered with
686 halocarbon oil 700 (Sigma-Aldrich). Glass capillaries (2-000-075; Drummond) were
687 prepared in advance by pulling with a puller (PN-3; Narishige). The capillary tip was
688 broken using forceps, just before use, and filled with lysis buffer supplied in Dynabeads
689 mRNA DIRECT Kit (Ambion) by capillary action. Upon the manual manipulation of
690 the capillary under the stereomicroscope, approximately 10–30 cells were sucked from
691 a central, an intermediate, or a peripheral region of the stage-3 embryo and transferred
692 into 0.2 ml tubes containing 10 µl of lysis buffer. The samples were stored at -80 °C
693 until they were retrieved for RNA extraction.

694

695 **RNA-seq of isolated cells**

696 Poly(A) mRNA was extracted using the Dynabeads mRNA DIRECT Kit (Ambion).
697 After fragmentation of the extracted RNA for 5 min at 94 °C, first-strand cDNA
698 synthesis and subsequent cDNA amplification by 22 cycles of polymerase chain
699 reaction (PCR) were performed using the SMARTer stranded RNA-seq kit (Takara).
700 The synthesized first-strand cDNA and amplified cDNA were purified using Ampure
701 XP Beads (Beckman Coulter). Constructed libraries for sequencing were quantified
702 using the Agilent 2100 BioAnalyzer high sensitivity DNA kit (Agilent). Two or three
703 libraries for each region of the stage-3 embryo were sequenced in single-end runs in

the antisense direction using the MiSeq reagent kit V3 (150 cycles) on the Illumina MiSeq platform. Over 10 million reads were obtained from each library. Following essentially the same procedure, RNA-seq of cells from central and peripheral regions of stage 4 and 5 embryos was performed.

Processing of RNA-seq data

The adapter and primer sequences, as well as the first three bases derived from the SMARTer Stranded Oligo, were trimmed from the MiSeq raw reads using CLC Genomics Workbench 7.0.3 (Qiagen). Quality trimming was also performed at the following parameter settings: quality score, limit = 0.05; trim ambiguous nucleotides, maximum number of ambiguities = 2; and filter on length, discard reads below length = 30. Trimmed reads were aligned to the *Parasteatoda tepidariorum* genome (Ptep_1.0, GCA_000365465.1) using the BLAT algorithm [86] in the DNA Data Bank of Japan (DDBJ) Read Annotation Pipeline (https://p.ddbj.nig.ac.jp/pipeline/). Output alignments were filtered using the PERL script filterPSL.pl, which is accessible from the AUGUSTUS 3.0.1 scripts folder (http://github.com/Gaius-Augustus/Augustus), with the following settings: 60% coverage; 90% identity; uniqueness threshold 0.96. The filtered alignments (pslx-format) were converted to sam-format. Based on these sam-format data, the number of mapped reads was counted against the AUGUSTUS gene models (aug3.1; https://i5k.nal.usda.gov/content/data-downloads)[31]) using htseq-count v.0.6.1p1 [87] with default settings. The RNA-seq datasets, including the gene count matrix, were deposited in the NCBI Gene Expression Omnibus (GEO) database (GSE193511).

Comparative analyses of RNA-seq gene count datasets

To assess the consistency of RNA-seq gene count datasets between biological replicates of each sample group, the coefficients of determination were calculated using the gene count matrix, and confirmed to be exceed 0.85. Out of the 27,990 annotated genes, 10,862 genes showed one or more counts per million (cpm) for at least one of the eight samples (p1-p3, i1-i3, c1, and c2). Count data matrices on these genes (10,862 genes × 8 samples) were used for comparative analyses. Differentially expressed genes (DEGs) were identified using a Bioconductor package edgeR (version 3.8.6) [49]. The

following three types of comparisons were set up: comparison I, c1 and c2 vs. p1-p3 and i1-i3; comparison II, p1-p3 vs. c1, c2, and i1-i3; and comparison III, i1-i3 vs. c1, c2, and p1-p3. Two criteria were applied to determine the high-priority candidate genes: first, $\log_2$FC < -10 in comparisons I and II, and $\log_2$FC > 10 in comparison III; and second, lower FDR values.

cDNA cloning

Full-length or partial cDNAs of newly identified genes were obtained from our collections of expressed sequence tag clones previously described [32,39], or were isolated by PCR amplification. cDNA fragments cloned in pBluescript II SK(+) (Agilent), pTriplEx2 (Takara) or pZL1 (Invitrogen) were used to synthesize dsRNA for pRNAi and/or RNA probes for in situ hybridization. The primers and cDNA clones used are summarized in Table S16 (Additional file 12).

Parental RNAi

For dsRNA synthesis, DNA templates with the T7 promoter sequence at both ends were prepared by PCR using appropriate primers depending on the plasmid type used. dsRNAs were synthesized using a Megascript Kit (Ambion) as described previously [29]. One to two µl of the dsRNA solution at a concentration of 2.0 µg/µl was injected into the abdomen of adult females four times at 2–3 day-intervals using pulled glass capillary tubes. In the pilot pRNAi screen, dsRNA against each gene was injected into two or four females. When egg laying took place, more than 10 eggs were randomly selected from each egg sac and transferred into halocarbon oil 700, which allowed us to nondestructively monitor the embryonic development through cleared chorion.

For three genes (*g26874*, *g7720*, *g4238*) that were judged as positive in the pilot screen, 2 or 3 additional dsRNAs were prepared from non-overlapping regions of each of the cDNAs, and each dsRNA was injected into at least 2 females. Development of eggs laid by the injected females were monitored using time-lapse recording, or with occasional visual inspection, under the stereo microscope. *gfp* dsRNA was used as the control.

Time-lapse microscopy of live embryos

Embryos dechorionated with 50 % commercial bleach were placed on a glass slide with double-sticky tape and covered with halocarbon oil 700. When the observation was started from stage 1, the dechorionation step was omitted to prevent possible effect on the development. Images were taken every 5 or 10 min using a stereo microscope (SZX12, Olympus) equipped with a color CCD camera (C7780-10, Hamamatsu Photonics) controlled by AquaCosmos software (Hamamatsu Photonics) or other stereo microscopes (M165C, Leica; or SZX7, Olympus) equipped with a color CMOS camera (WRAYCAM-G200 or -NF300, WRAYMER).

For live imaging of nuclei around the germ-disc/non-germ-disc transition area, dechorionated stage-4 embryos were placed on a glass slide with double-sticky tape, and an embryo appropriately oriented was selected and skewered with a thin glass needle to prevent the embryo from rotating during later development. A 1,000× stock solution of a cell-permeable dye SPY555-DNA (Spirochrome), which was prepared in 50 µl of dimethylsulfoxide, was microinjected into the perivitelline space of the skewered egg. The injecting volume should be low to avoid affecting the development of the embryo from being affected. Approximately 1 hour after dye injection, the embryo started to be examined under an Olympus BX50 fluorescence microscope equipped with a cooled CCD camera (CoolSNAP HQ, Roper Scientific) controlled by MetaMorph.version 6.1 (Universal Imaging). Using 10 × objective lens (UPlanAPO 10×/0.40, Olympus), bright-field and fluorescence 500 × 500 pixel images were acquired every 5 min at exposure times of 10 msec and 100 msec, respectively. To reduce the excitation light, two neutral density filters (U-ND6-2 and U-ND25-2, Olympus) were used. A single focal plane, which was manually adjusted during approximately 30 h of observation, was recorded at each time point. The observed embryo was checked for its normal development. Time-lapse images were analyzed using Imaris version 7.6.5, where cells were manually tracked, and ImageJ version 1.51d.

Molecular phylogenetic analysis of GATA family members

To collect amino acid sequences containing GATA-type DNA binding domain from many arachnid species and other arthropod and nonarthropod metazoan representative species, we used nucleotide sequence resources presented in Table S7 (Additional file

7), which included coding sequences from sequenced genomes, transcriptome assemblies, and RNA-seq raw data, retrieved from GenBank (NCBI) or GigaScience database. RNA-seq of *Hasarius adansoni* mid-stage embryos was performed in this study, as described below. The RNA-seq data were subjected to de novo assembling using Trinity (version 2.11.0). To identify amino acid sequences coding for GATA-type DNA binding domains in the retrieved or assembled nucleotide sequences, blastp searches were performed using the Fuchi amino acid sequence as a query with a cut-off e-value of 1e-2, followed by the systematic selection of sequences that contained at least one GATA-type zinc-finger motif sequence ($CX_2CX_{16-20}CX_2C$). The identified amino acid sequences were manually aligned and classified based on the detection of signature sequences, excluding GATA-like proteins that had only one GATA-type zinc finger motif. For molecular phylogenetic analysis, 75 amino acid sites from 118 sequences, which were unambiguously aligned, were used (Additional file 7: Table S8). The molecular phylogeny was inferred using the Maximum Likelihood (ML) method and JTT matrix-based model [88] on the software MEGA11 [89].

RNA-seq of whole embryos

For RNA-seq analyses of *fuchi* pRNAi embryos, mated adult females were injected with approximately 1–2 µl of *fuchi* dsRNA solution (2 µg/µl) four times at 2- to 3-day intervals. For RNA extraction, 50–100 embryos at stage 2, 3, and early stage 5 that were derived from egg sacs produced by the injected females 2 days before (untreated) and 18–19 days after the first injection of the dsRNA were used. Two biological replicates were prepared for each sample type. The mRNA extraction and library construction for sequencing were performed as previously described [36]. The libraries were quantified using the Library quantification kit (Takara) and Thermal cycler Dice Realtime TP800 (Takara) and sequenced in single-end runs (150 cycles) in the antisense direction on the Illumina MiSeq platform. The sequence reads were processed as previously described [36], and the datasets were deposited in the GEO database (GSE193650). Estimates of DEGs between untreated and *fuchi* pRNAi embryos at each stage were performed using EdgeR (version 3.8.6).

For the *H. adansoni* RNA-seq, poly(A) mRNA was extracted using a QuickPrep Micro mRNA purification kit (GE Healthcare) from 20 sibling mid-stage

832 embryos with extending limbs. Library construction for sequencing was performed as
833 previously described [36]. The library was sequenced in a paired-end run (150 × 2
834 cycles) on the Illumina Miseq platform, and the raw reads (SRR17326784) and the *H.*
835 *adansoni* transcriptome assembly (GJQJ00000000) were deposited in GenBank.
836
837 **ATAC-seq of whole embryos**
838 ATAC-seq was performed following the procedure described by Buenrostro et al.
839 (2015) [90] with modifications considering the procedure reported by Haines and
840 Eisen (2018) [91]. In brief, 40 whole embryos at stage 3 (18 h AEL) were
841 homogenized using disposable pellet pestles (12-141-368; Fisher Scientific) and 1.5
842 mL Eppendorf tubes (0030125150) in 50 µl lysis buffer (10mM Tris, 10mM NaCl,
843 3mM $MgCl_2$, adjusted to pH 7.4 with HCl) containing 0.15 mM spermidine, after
844 which 50 µl of lysis buffer and 1 µl of 10% Nonidet P-40 were added as the pestle
845 was rinsed. After a 10 min incubation, nuclei were spun down at 800 g and
846 resuspended in 17.5 µl water, followed by the addition of 25 µl of 2× TD buffer
847 (Illumina) and 7.5 µl of Nextra Tn5 transposase (Illumina). Transposed DNA was
848 purified using MinElute Reaction Cleanup Kit (Qiagen) and amplified with Illumina
849 Nextera Transposase Adaptors index PCR primers, and the amplified DNA was
850 purified using Ampure XP Beads (Beckman Coulter). Constructed libraries were
851 paired-end sequenced (151 bp reads × 2) on the Illumina HiSeq X Ten system.
852 Comparative analyses of ATAC-seq datasets from three different sample
853 types (wild-type, *fuchi* pRNAi, and *Pt-hh* pRNAi) were performed basically
854 following the procedure described by Reske et al. (2020)[92] with slight
855 modifications based on guidelines provided by Gaspar (2019)[93] and Delisle et al.
856 (2021)[94]. Two biological replicates were obtained from each sample type. ATAC-
857 seq raw reads were trimmed for adaptor and primer sequences and low-quality
858 sequences using Trim Galore! with default settings. Trimmed reads were then aligned
859 to the *P. tepidariorum* genome (Ptep_2.0) using bowtie2 v2.2.5 with default settings.
860 Reads mapped with low quality scores (less than 30) were removed using samtools
861 (version 1.9). PCR duplicates were removed using Picard MarkDuplicates (version
862 2.23.4). The alignments of filtered reads to the genome were saved as bam files. Peak
863 calling was performed using the ATAC-seq mode of Genrich (version 6.0).

Differential accessibility analysis was performed using a Bioconductor package, *csaw* [95]. Peak regions called in both replicates of each sample type were extracted, and the peak regions extracted from the three sample types were merged. Reads were counted in peaks, with low abundance peaks (log CPM < -3) removed. Read counts were subject to normalization with the trimmed mean of *M* values (TMM) method [96]. Differential accessibility was estimated using the glmQLFit and glmQLFTest functions in EdgeR (version 3.32.0). Peaks with FDR < 0.05 were considered as significant. To discover motif sequences in the identified differential peak regions, STREME [97] was used.

Wild-type whole embryos at stages 1 (9 h AEL) and 2 (12 h AEL) were similarly analyzed by ATAC-seq to detect genomic regions differentially accessible between the different stages (stages 1 to 3), but no clear results were obtained. All the ATAC-seq datasets were deposited in the GEO database (GSE193870).

Staining of embryos

Antisense RNA probes for in situ hybridization were prepared by *in vitro* transcription using Digoxigenin- or Dinitrophenyl-conjugated UTP (DIG, Roche 11277073910; DNP, PerkinElmer NEL555001EA) as previously described [56]. Whole-mount in situ hybridization with chromogenic substrate was performed in the previously described manner [29] with the exception of an additional tyramide-based signal amplification (TSA) process described previously [56]. In brief, after washing DIG-conjugated RNA probes, the samples were incubated with anti-DIG-POD antibody (11633716001, Roche; 1:500 dilution) and then reacted with DNP-tyramide (NEL747, PerkinElmer). In the detection step, anti-DNP-AP antibody (MB-3100, Vector; 1:50) and NBT/BCIP were used. Most samples were counterstained with 4',6-diamidino-2-phenylindole (DAPI; Sigma-Aldrich).

Double-color FISH was performed as previously described [56]. To visualize the DIG- and DNP-conjugated probes, anti-DIG-POD (Roche 11633716001; 1:500) and anti-DNP-HRP (PerkinElmer FP1129; 1:100) were used in combination with DyLight488-tyramide and DyLight680-tyramide, respectively.

Single- and double-color FISH were combined with immunostaining for β-catenin in certain cases (Figs. 5 and 6), where Proteinase K treatment prior to

hybridization was omitted. After completing the FISH procedure, the embryos were incubated with rabbit anti-β-catenin antibody (C2206, Sigma-Aldrich 1:500) and then with Cy3-conjugated anti-rabbit IgG antibody (AP187C, Chemicon; 1:200), followed by counterstaining with DAPI.

Image acquisition and processing

Images for chromogenically stained WISH samples were obtained using a stereo microscope (SZX12, Olympus), a fluorescence unit BT-ExSMOP (Biotools), and a CCD camera (C7780-10, Hamamatsu Photonics). For confocal microscopy of fluorescently stained embryos, the whole embryos were individually mounted on glass slides with spacers of approximately 100–500 µm, which were adjusted depending on the sample using sticky tape (CT-18S, Nichiban) and silicone vacuum grease (335148, Beckman). To view different sides of a single embryo, it was rotated after being mounted on the glass slide. The embryos were examined using a Leica TCS SPE confocal system equipped with four laser sources (405, 488, 532, and 635 nm), which were used to excite DAPI, DyLight488, Cy3, and DyLight680, respectively. Acquired confocal stacks were processed and analyzed using Imaris version 7.6.5 (Bitplane) and ImageJ version 1.51d. The Imaris snapshot feature and oblique slicer tool were used to obtain images capturing the embryonic regions of interest. Linear signals of cell-cell adherens junctions visualized by β-catenin staining were traced in Adobe Photoshop CS5 ver. 12.0.4.

Availability of data and materials

Raw and processed data for the comparative RNA-seq and ATAC-seq analyses are accessible from NCBI GEO (GSE193511, GSE193650, and GSE193870). The data aligned to the reference genome can be viewed on our web database (https://www.brh2.jp). The nucleotide sequences determined for *fuchi* and *Pt-GATA5* are available under the accessions LC671429 and LC671430 in the DDBJ/EMBL/GenBank International Nucleotide Sequence Databases. The sources of sequence data used in the molecular phylogenetic analysis are listed in Additional file 7: Tables S7 and S8. Supplementary movies showing the pilot pRNAi screen and the pRNAi specificity validation are available on figshare [50].

928

929 **Abbreviations**

930 ***AEL:*** After egg laying

931 ***ATAC-seq:*** Assay for transposase-accessible chromatin using sequencing

932 ***BR:*** Basic region

933 ***CPM:*** Counts per million

934 ***DAPI:*** 4',6-diamidino-2-phenylindole

935 ***DDBJ:*** DNA Data Bank of Japan

936 ***DEG:*** Differentially expressed gene

937 ***dsRNA:*** Double stranded RNA

938 ***FC:*** Fold change

939 ***FDR:*** False discovery rate

940 ***GEO:*** Gene Expression Omnibus

941 ***ML:*** Maximum likelihood

942 ***NCBI:*** National Center for Biotechnology Informataion

943 ***PCR:*** Polymerase chain reaction

944 ***pRNAi:*** Parental RNA interference

945 ***RNA-seq:*** RNA sequencing

946 ***RPKM:*** reads per kilobase of transcript, per million mapped reads

947 ***WISH:*** Whole-mount in situ hybridization

948 ***ZF:*** Zinc finger

949

950 **Acknowledgements**

951 We thank Akiko Noda for technical assistance, and other members of JT Biohistory

952 Research Hall for discussion.

953

954 **Funding**

955 This work was supported by JSPS Kakenhi (26440130, 17K07418, 20K06676 to YA;

956 15K07139 to HO), JST PRESTO (JPMJPR2041 to YA), and the core budget of JT

957 Biohistory Research Hall.

958

959 **Contributions**

S.I., Y.A., and H.O. designed the study. S.I. created all the RNA-seq datasets. S.I. analyzed the RNA-seq datasets with help from Y.A. S.I. performed the pRNAi screen and the gene expression and phenotype analyses. S.I. and H.O. performed the phylogenetic analysis. R.N. created the ATAC-seq datasets. R.N. analyzed the ATAC-seq datasets with help from Y.A. and H.O. S.I. wrote the first draft of the manuscript. H.O. wrote the final version of the manuscript with input from all authors.

Ethics approval and consent to participate

Not applicable

Consent for publication

Not applicable

Competing interests

The authors declare that they have no competing interests.

Supplementary Information

Additional file 1: Movie S1. Time-lapse video of sibling *Parasteatoda tepidariorum* embryos. The left embryo is the same as shown in Figure 1. Time after egg laying (AEL) is indicated. Scale bar, 100 μm.

Additional file 2: Table S1. List of DEG candidates identified by comparative transcriptome analysis of c versus i/p cells from stage-3 embryo (comparison I). **Table S2.** List of DEG candidates identified by comparative transcriptome analysis of p versus c/i cells from stage-3 embryo (comparison II)**. Table S3.** List of DEG candidates identified by comparative transcriptome analysis of i versus c/p cells from stage-3 embryo (comparison III)**. Table S4.** List of DEG candidates indentified by comparative transcriptome analysis of c versus p cells from stage-4 embryo**. Table S5.** List of DEG candidates identified by comparative transcriptome analysis of c versus p cells from early stage-5 embryo.

Additional file 3: Figure S1. Chromogenic WISH of stage-3 embryos using probes for 19 selected DEG candidates. **Figure S2.** Validation of the specificity of the RNAi effects for *g26874*, *g7720*, and *g4238*. **Figure S3.** Developmental transcript profiling

992 of *P. tepidariorum* GATA family genes in wild-type embryos. **Figure S4.** Cell counting
993 in a stage-3 embryo stained for *fuchi*. **Figure S5.** *fuchi* expression in pEND cells.
994 **Figure S6.** Characterization of 5 DEG candidates from the comparative transcriptome
995 analysis of stage-2 *fuchi* pRNAi versus untreated embryos. **Figure S7.** Characterization
996 of the top-10 DEG candidates from the comparative transcriptome analysis of stage-3
997 *fuchi* pRNAi versus untreated embryos. **Figure S8.** Effects of *fuchi* RNAi on
998 expression of selected genes. **Figure S9.** Single-nucleus transcriptome data showing
999 endodermal and mesodermal cell populations in late stage-5 embryos. **Figure S10.**
1000 Single-nucleus and single-cell transcriptome data showing cell populations expressing
1001 the genes regulated by *fuchi*.
1002 **Additional file 4: Table S6.** Summary of a pilot pRNAi screen of 19 selected genes.
1003 **Additional file 5: Movie S2.** Time-lapse video showing phenotypes *gfp*, *g26874*,
1004 *g7720*, and *g4238* pRNAi embryos. Time after egg laying (AEL) and time after start of
1005 recording are indicated. Movie starts are adjusted by the timing of blastoderm
1006 formation. Some of the embryos are the same as those shown in Figure 3A. Scale bar,
1007 100 µm.
1008 **Additional file 6: Movie S3.** Tracking of cells in wild-type and *g26874* pRNAi
1009 embryos. In the *g26874* pRNAi embryo, cells on the abembryonic side initially shift
1010 toward forming a germ disc but, later, they return back. Time after start of recording is
1011 indicated.
1012 **Additional file 7: Table S7.** List of bioinformatic resources used for phylogenetic
1013 characterization of Fuchi and other GATA family members in spiders. **Table S8.** Amino
1014 acid sequence alignment and classification of GATA family members from spiders and
1015 other metazoans.
1016 **Additional file 8: Movie S4.** Time-lapse video showing cell internalizations taking
1017 place around the germ-disc rim. Nuclei labeled by SPY555-DNA are presented in white.
1018 The germ disc on the embryonic side is to the lower right, while the non-germ-disc
1019 region on the abembryonic side is to the upper left. Internalizing cells are tracked. Cells
1020 from the non-germ-disc region are moving to below the germ-disc epithelium. Later,
1021 cells at the germ-disc rim internalize. Time [d : h : m] after start of recording is indicated.
1022 **Additional file 9: Table S9.** List of DEGs identified by comparative transcriptome
1023 analysis of *fuchi* pRNAi versus untreated embryos at stage 2. **Table S10.** List of DEGs

identified by comparative transcriptome analysis of *fuchi* pRNAi versus untreated embryos at stage 3. **Table S11.** List of DEGs identified by comparative transcriptome analysis of *fuchi* pRNAi versus untreated embryos at early stage 5.

Additional file 10: Table S12. Data from comparative analysis of read counts in extracted ATAC-seq peaks between *fuchi* pRNAi and wild-type embryos at stage 3 using edgeR. **Table 13.** List of differential ATAC-seq peaks between *fuchi* pRNAi and wild-type embryos at stage 3 (FDR < 0.05).

Additional file 11: Table S14. Data from comparative analysis of read counts in extracted ATAC-seq peaks between *Pt-hh* pRNAi and wild-type embryos at stage 3 using edgeR. **Table S15.** List of differential ATAC-seq peaks between Pt-hh pRNAi and wild-type embryos at stage 3 (FDR < 0.05).

Additional file 12: Table S16. Primers and cDNA clones used for RNAi and in situ hybridization.

References

1. Raff RA. The Shape of Life: Genes, Development, and the Evolution of Animal Form. Chicago: Univ. Chicago Press; 1996.

2. Duboule D. Temporal colinearity and the phylotypic progression: a basis for the stability of a vertebrate Bauplan and the evolution of morphologies through heterochrony. Dev Suppl. 1994;135–42.

3. Galis F, van Dooren TJM, Metz JAJ. Conservation of the segmented germband stage: robustness or pleiotropy? Trends Genet. 2002;18:504–9.

4. Sander K. The evolution of patterning mechanisms: gleanings from insect embryogenesis and spermatogenesis. In: Goodwin BC Hold N Wylie CC. (eds) Development and evolution. Cambridge: Cambridge University Press; 1983. p. 137–60.

5. Kalinka AT, Varga KM, Gerrard DT, Preibisch S, Corcoran DL, Jarrells J, et al. Gene expression divergence recapitulates the developmental hourglass model. Nature. 2010;468:811–4.

6. Richardson MK. Heterochrony and the Phylotypic Period. Dev Biol. 1995;172:412–21.

7. Irie N, Kuratani S. Comparative transcriptome analysis reveals vertebrate phylotypic period during organogenesis. Nat Commun. 2011;2:248.

1053 8. Domazet-Loso T, Tautz D. An Evolutionary Analysis of Orphan Genes in Drosophila. Genome Res.
1054 2003;13:2213–9.

1055 9. Khalturin K, Hemmrich G, Fraune S, Augustin R, Bosch TCG. More than just orphans: are
1056 taxonomically-restricted genes important in evolution? Trends in Genetics. 2009;25:404–13.

1057 10. Thomas GWC, Dohmen E, Hughes DST, Murali SC, Poelchau M, Glastad K, et al. Gene content
1058 evolution in the arthropods. Genome Biol. 2020;21:15.

1059 11. Morino Y, Hashimoto N, Wada H. Expansion of TALE homeobox genes and the evolution of
1060 spiralian development. Nat Ecol Evol. 2017;1:1942–9.

1061 12. Holland LZ, Albalat R, Azumi K, Benito-Gutiérrez È, Blow MJ, Bronner-Fraser M, et al. The
1062 amphioxus genome illuminates vertebrate origins and cephalochordate biology. Genome Res.
1063 2008;18:1100–11.

1064 13. Khalturin K, Anton-Erxleben F, Sassmann S, Wittlieb J, Hemmrich G, Bosch TCG. A Novel Gene
1065 Family Controls Species-Specific Morphological Traits in Hydra. PLOS Biol. Public Library of Science;
1066 2008;6:e278.

1067 14. Stauber M, J\textbackslashHackle H, Schmidt-Ott U. The anterior determinant bicoid of Drosophila
1068 is a derived Hox class 3 gene. Proc Natl Acad Sci U A. 1999;96:3786–9.

1069 15. Lynch JA, Peel AD, Drechsler A, Averof M, Roth S. EGF signaling and the origin of axial polarity
1070 among the insects. Curr Biol. 2010;20:1042–7.

1071 16. Lima LF, Torres AQ, Jardim R, Mesquita RD, Schama R. Evolution of Toll, Spatzle and MyD88 in
1072 insects: the problem of the Diptera bias. BMC Genomics. 2021;22:562.

1073 17. Nishida H, Sawada K. macho-1 encodes a localized mRNA in ascidian eggs that specifies muscle
1074 fate during embryogenesis. Nature. 2001;409:724–9.

1075 18. Fekany K, Yamanaka Y, Leung T, Sirotkin HI, Topczewski J, Gates MA, et al. The zebrafish bozozok
1076 locus encodes Dharma, a homeodomain protein essential for induction of gastrula organizer and
1077 dorsoanterior embryonic structures. Development. 1999;126:1427–38.

1078 19. Bae S, Reid CD, Kessler DS. Siamois and Twin are redundant and essential in formation of the
1079 Spemann organizer. Dev Biol. 2011;352:367–81.

1080 20. Pultz MA, Zimmerman KK, Alto NM, Kaeberlein M, Lange SK, Pitt JN, et al. A Genetic Screen for
1081 Zygotic Embryonic Lethal Mutations Affecting Cuticular Morphology in the Wasp Nasonia vitripennis.
1082 Genetics. 2000;154:1213–29.

1083 21. Sulston IA, Anderson KV. Embryonic patterning mutants of Tribolium castaneum. Development.
1084 1996;122:805–14.

1085 22. Maderspacher F, Bucher G, Klingler M. Pair-rule and gap gene mutants in the flour beetle Tribolium
1086 castaneum. Dev Genes Evol. 1998;208:558–68.

1087 23. Schmitt-Engel C, Schultheis D, Schwirz J, Ströhlein N, Troelenberg N, Majumdar U, et al. The
1088 iBeetle large-scale RNAi screen reveals gene functions for insect development and physiology. Nat
1089 Commun. 2015;6:7822.

1090 24. Consortium i5K. The i5K Initiative: advancing arthropod genomics for knowledge, human health,
1091 agriculture, and the environment. J Hered. 2013;104:595–600.

1092 25. Oda H, Akiyama-Oda Y. The common house spider Parasteatoda tepidariorum. EvoDevo. 2020;11:6.

1093 26. Kanayama M, Akiyama-Oda Y, Oda H. Early embryonic development in the spider Achaearanea
1094 tepidariorum: microinjection verifies that cellularization is complete before the blastoderm stage.
1095 Arthropod Struct Dev. 2010;39:436–45.

1096 27. Suzuki H, Kondo A. Early embryonic development, including germ-disk stage, in the Theridiid
1097 spider Achaearanea japonica (Bös. et Str.). J Morphol. 1995;224:147–57.

1098 28. Akiyama-Oda Y, Oda H. Early patterning of the spider embryo: a cluster of mesenchymal cells at
1099 the cumulus produces Dpp signals received by germ disc epithelial cells. Development. 2003;130:1735–
1100 47.

1101 29. Akiyama-Oda Y, Oda H. Axis specification in the spider embryo: dpp is required for radial-to-axial
1102 symmetry transformation and sog for ventral patterning. Development. 2006;133:2347–57.

1103 30. Akiyama-Oda Y, Oda H. Cell migration that orients the dorsoventral axis is coordinated with
1104 anteroposterior patterning mediated by Hedgehog signaling in the early spider embryo. Development.
1105 2010;137:1263–73.

1106 31. Schwager EE, Sharma PP, Clarke T, Leite DJ, Wierschin T, Pechmann M, et al. The house spider
1107 genome reveals an ancient whole-genome duplication during arachnid evolution. BMC Biol. 2017;15:62.

1108 32. Oda H, Nishimura O, Hirao Y, Tarui H, Agata K, Akiyama-Oda Y. Progressive activation of Delta-
1109 Notch signaling from around the blastopore is required to set up a functional caudal lobe in the spider
1110 Achaearanea tepidariorum. Development. 2007;134:2195–205.

1111 33. Posnien N, Zeng V, Schwager EE, Pechmann M, Hilbrant M, Keefe JD, et al. A comprehensive
1112 reference transcriptome resource for the common house spider Parasteatoda tepidariorum. PLoS One.
1113 2014;9:e104885.

1114 34. Kono N, Nakamura H, Ito Y, Tomita M, Arakawa K. Evaluation of the impact of RNA preservation
1115 methods of spiders for de novo transcriptome assembly. Mol Ecol Resour. 2016;16:662–72.

1116 35. Sasaki M, Akiyama-Oda Y, Oda H. Evolutionary origin of type IV classical cadherins in arthropods.
1117 BMC Evol Biol. 2017;17:142.

1118 36. Iwasaki-Yokozawa S, Akiyama-Oda Y, Oda H. Genome-scale embryonic developmental profile of
1119 gene expression in the common house spider Parasteatoda tepidariorum. Data Brief. 2018;19:865–7.

1120 37. Pechmann M. Formation of the germ-disc in spider embryos by a condensation-like mechanism.
1121 Front Zool. 2016;13:35.

1122 38. Hemmi N, Akiyama-Oda Y, Fujimoto K, Oda H. A quantitative study of the diversity of stripe-
1123 forming processes in an arthropod cell-based field undergoing axis formation and growth. Dev Biol.
1124 2018;437:84–104.

1125 39. Kanayama M, Akiyama-Oda Y, Nishimura O, Tarui H, Agata K, Oda H. Travelling and splitting of
1126 a wave of hedgehog expression involved in spider-head segmentation. Nat Commun. 2011;2:500.

1127 40. Akiyama-Oda Y, Oda H. Hedgehog signaling controls segmentation dynamics and diversity via
1128 msx1in a spider embryo. Sci Adv. 2020;6.

1129 41. Montgomery J TH. The development of Theridium, an Aranead, up to the stage of reversion. J
1130 Morphol. 1909;20:297–352.

1131 42. Chaw RC, Vance E, Black SD. Gastrulation in the spider Zygiella x-notata involves three distinct
1132 phases of cell internalization. Dev Dyn. 2007;236:3484–95.

1133 43. Mittmann B, Wolff C. Embryonic development and staging of the cobweb spider Parasteatoda
1134 tepidariorum C. L. Koch, 1841 (syn.: Achaearanea tepidariorum; Araneomorphae; Theridiidae). Dev
1135 Genes Evol. 2012;222:189–216.

1136 44. Edgar A, Bates C, Larkin K, Black S. Gastrulation occurs in multiple phases at two distinct sites in
1137 Latrodectus and Cheiracanthium spiders. Evodevo. 2015;6:33.

1138 45. Wolff C, Hilbrant M. The embryonic development of the central American wandering spider
1139 Cupiennius salei. Front Zool. 2011;8:15.

1140 46. Turetzek N, Prpic N-MM. Observations on germ band development in the cellar spider Pholcus
1141 phalangioides. Dev Genes Evol. 2016;226:413–22.

1142 47. Pechmann M. Embryonic development and secondary axis induction in the Brazilian white knee
1143 tarantula Acanthoscurria geniculata, C. L. Koch, 1841 (Araneae; Mygalomorphae; Theraphosidae). Dev
1144 Genes Evol. 2020;230:75–94.

1145 48. Sekiguchi K. Reduplication in spider eggs produced by centrifugation. Sci Rep Tokyo Bunrika
1146 Daigaku Sec B. 1957;8:227–80.

1147 49. Robinson MD, McCarthy DJ, Smyth GK. edgeR: a Bioconductor package for differential expression
1148 analysis of digital gene expression data. Bioinformatics. 2010;26:139–40.

1149 50. Iwasaki-Yokozawa S, Akiyama-Oda Y, Oda H. Supplementary movies for “Lineage-specific, fast-
1150 evolving GATA-like gene regulates zygotic gene activation to promote endoderm specification and
1151 pattern formation in the Theridiidae spider” [Internet]. figshare. 2022 [cited 2022 Jun 8]. Available from:
1152 https://doi.org/10.6084/m9.figshare.c.5963661.v1

1153 51. Su Y, Song Y, Wang Y, Jessop L, Zhan L, Stumph WE. Characterization of a Drosophila Proximal-
1154 Sequence-Element-Binding Protein Involved in Transcription of Small Nuclear RNA Genes. Eur J
1155 Biochem. 1997;248:231–7.

1156 52. Chen T, Bunting M, Karim FD, Thummel CS. Isolation and characterization of five Drosophila genes
1157 that encode an ets-related DNA binding domain. Dev Biol. 1992;151:176–91.

1158 53. Pechmann M, Benton MA, Kenny NJ, Posnien N, Roth S. A novel role for Ets4in axis specification
1159 and cell migration in the spider Parasteatoda tepidariorum. Elife. 2017;6.

1160 54. Tang Y, Wei Y, He W, Wang Y, Zhong J, Qin C. GATA transcription factors in vertebrates:
1161 evolutionary, structural and functional interplay. Mol Genet Genomics. 2014;289:203–14.

1162 55. Patient RK, McGhee JD. The GATA family (vertebrates and invertebrates). Curr Opin Genet Dev.
1163 2002;12:416–22.

1164 56. Akiyama-Oda Y, Oda H. Multi-color FISH facilitates analysis of cell-type diversification and
1165 developmental gene regulation in the Parasteatoda spider embryo. Dev Growth Differ. 2016;58:215–24.

1166 57. Oda H, Akiyama-Oda Y. Microarray data on the comparison of transcript expression between normal
1167 and Pt-DeltaRNAi embryos in the common house spider Parasteatoda tepidariorum. Data Brief.
1168 2019;25:104350.

1169 58. Yamazaki K, Akiyama-Oda Y, Oda H. Expression patterns of a twist-related gene in embryos of the
1170 spider Achaearanea tepidariorum reveal divergent aspects of mesoderm development in the fly and
1171 spider. Zool Sci. 2005;22:177–85.

1172 59. Iwafuchi-Doi M, Zaret KS. Pioneer transcription factors in cell reprogramming. Genes Dev.
1173 2014;28:2679–92.

1174 60. Akiyama-Oda Y, Akaiwa T, Oda H. Reconstruction of the Global Polarity of an Early Spider Embryo
1175 by Single-Cell and Single-Nucleus Transcriptome Analysis. submitted.

1176 61. Rebagliati MR, Weeks DL, Harvey RP, Melton DA. Identification and cloning of localized maternal
1177 RNAs from xenopus eggs. Cell. 1985;42:769–77.

1178 62. Sasai Y, Lu B, Steinbeisser H, Geissert D, Gont LK, De Robertis EM. Xenopus chordin: a novel
1179 dorsalizing factor activated by organizer-specific homeobox genes. Cell. 1994;79:779–90.

1180 63. Kozhemyakina E, Ionescu A, Lassar AB. GATA6 is a crucial regulator of Shh in the limb bud. PLoS
1181 Genet. 2014;10:e1004072.

64. Tokusumi Y, Tokusumi T, Stoller-Conrad J, Schulz RA. Serpent, Suppressor of Hairless and U-shaped are crucial regulators of hedgehog niche expression and prohemocyte maintenance during Drosophila larval hematopoiesis. Development. 2010;137:3561–8.

65. Xuan S, Sussel L. GATA4 and GATA6 regulate pancreatic endoderm identity through inhibition of hedgehog signaling. Development. 2016;143:780–6.

66. Fujikura J, Yamato E, Yonemura S, Hosoda K, Masui S, Nakao K, et al. Differentiation of embryonic stem cells is induced by GATA factors. Genes Dev. 2002;16:784–9.

67. Tremblay M, Sanchez-Ferras O, Bouchard M. GATA transcription factors in development and disease. Development. 2018;145:dev164384.

68. Gillis WQ, Bowerman BA, Schneider SQ. The evolution of protostome GATA factors: molecular phylogenetics, synteny, and intron/exon structure reveal orthologous relationships. BMC Evol Biol. 2008;8:112.

69. Reuter R. The gene serpent has homeotic properties and specifies endoderm versus ectoderm within the Drosophila gut. Development. 1994;120:1123–35.

70. Morrisey EE, Tang Z, Sigrist K, Lu MM, Jiang F, Ip HS, et al. GATA6 regulates HNF4 and is required for differentiation of visceral endoderm in the mouse embryo. Genes Dev. 1998;12:3579–90.

71. Shivdasani RA. Molecular Regulation of Vertebrate Early Endoderm Development. Dev Biol. 2002;249:191–203.

72. Tam PP, Kanai-Azuma M, Kanai Y. Early endoderm development in vertebrates: lineage differentiation and morphogenetic function. Curr Opin Genet Dev. 2003;13:393–400.

73. Fukuda K, Kikuchi Y. Endoderm development in vertebrates: fate mapping, induction and regional specification. Dev Growth Differ. 2005;47:343–55.

74. Frankenberg S, Gerbe F, Bessonnard S, Belville C, Pouchin P, Bardot O, et al. Primitive Endoderm Differentiates via a Three-Step Mechanism Involving Nanog and RTK Signaling. Dev Cell. 2011;21:1005–13.

1207 75. Heslop JA, Pournasr B, Liu J-T, Duncan SA. GATA6 defines endoderm fate by controlling chromatin
1208 accessibility during differentiation of human-induced pluripotent stem cells. Cell Rep. 2021;35:109145.

1209 76. Feitosa NM, Pechmann M, Schwager EE, Tobias-Santos V, McGregor AP, Damen WGM, et al.
1210 Molecular control of gut formation in the spider Parasteatoda tepidariorum. Genesis. 2017;55.

1211 77. Maduro MF, Rothman JH. Making Worm Guts: The Gene Regulatory Network of the Caenorhabditis
1212 elegans Endoderm. Dev Biol. 2002;246:68–85.

1213 78. Murakami R, Okumura T, Uchiyama H. GATA factors as key regulatory molecules in the
1214 development of Drosophila endoderm. Dev Growth Differ. 2005;47:581–9.

1215 79. Tsang AP, Visvader JE, Turner CA, Fujiwara Y, Yu C, Weiss MJ, et al. FOG, a Multitype Zinc Finger
1216 Protein, Acts as a Cofactor for Transcription Factor GATA-1 in Erythroid and Megakaryocytic
1217 Differentiation. Cell. 1997;90:109–19.

1218 80. Crispino JD, Lodish MB, MacKay JP, Orkin SH. Use of Altered Specificity Mutants to Probe a
1219 Specific Protein–Protein Interaction in Differentiation: the GATA-1:FOG Complex. Mol Cell.
1220 1999;3:219–28.

1221 81. Waltzer, Lucas, Bataille, Laetitia, Peyrefitte, Sandrine, Haenlin, Marc. Two isoforms of Serpent
1222 containing either one or two GATA zinc fingers have different roles in Drosophila haematopoiesis.
1223 EMBO J. 2002;21:5477–86.

1224 82. Chlon TM, Doré LC, Crispino JD. Cofactor-mediated restriction of GATA-1 chromatin occupancy
1225 coordinates lineage-specific gene expression. Mol Cell. 2012;47:608–21.

1226 83. Pedone, Paolo, V., Omichinski, James, G., Nony, Pascale, Trainor, Cecelia, Gronenborn, Angela, M.,
1227 Clore, G.Marius, et al. The N-terminal fingers of chicken GATA-2 and GATA–3 are independent
1228 sequence-specific DNA binding domains. EMBO J. 1997;16:2874–82.

1229 84. Oda H, Iwasaki-Yokozawa S, Usui T, Akiyama-Oda Y. Experimental duplication of bilaterian body
1230 axes in spider embryos: Holm's organizer and self-regulation of embryonic fields. Dev Genes Evol.
1231 2020;230:49–63.

1232 85. Holm Å. Experimentelle Untersuchungen über die Entwicklung und Entwicklungsphysiologie des
1233 Spinnenembryos. Zool BiDr Upps. 1952;29:293–424.

1234 86. Kent WJ. BLAT—The BLAST-Like Alignment Tool. Genome Res. 2002;12:656–64.

1235 87. Anders S, Pyl PT, Huber W. HTSeq—a Python framework to work with high-throughput sequencing
1236 data. Bioinformatics. 2015;31:166–9.

1237 88. Jones DT, Taylor WR, Thornton JM. The rapid generation of mutation data matrices from protein
1238 sequences. Bioinformatics. 1992;8:275–82.

1239 89. Tamura K, Stecher G, Kumar S. MEGA11: Molecular Evolutionary Genetics Analysis Version 11.
1240 Mol Biol Evol. 2021;38:3022–7.

1241 90. Buenrostro JD, Wu B, Chang HY, Greenleaf WJ. ATAC-seq: A Method for Assaying Chromatin
1242 Accessibility Genome-Wide. Curr Protoc Mol Biol. 2015;109:21.29.1-9.

1243 91. Haines JE, Eisen MB. Patterns of chromatin accessibility along the anterior-posterior axis in the
1244 early Drosophila embryo. PLoS Genet. 2018;14:e1007367.

1245 92. Reske JJ, Wilson MR, Chandler RL. ATAC-seq normalization method can significantly affect
1246 differential accessibility analysis and interpretation. Epigenetics Chromatin. 2020;13:22.

1247 93. Gaspar JM. ATAC-seq Guidelines [Internet]. Harv. FAS Inform. 2019 [cited 2022 Apr 26]. Available
1248 from: https://informatics.fas.harvard.edu/./atac-seq-guidelines.html

1249 94. Delisle, L., Doyle, M., Heyl, F. Galaxy Training: ATAC-Seq data analysis [Internet]. 2021 [cited
1250 2022 Apr 26]. Available from: https://training.galaxyproject.org/training-
1251 material/topics/epigenetics/tutorials/atac-seq/tutorial.html

1252 95. Lun ATL, Smyth GK. csaw: a Bioconductor package for differential binding analysis of ChIP-seq
1253 data using sliding windows. Nucleic Acids Res. 2016;44:e45.

1254 96. Robinson MD, Oshlack A. A scaling normalization method for differential expression analysis of
1255 RNA-seq data. Genome Biol. 2010;11:R25.

1256 97. Bailey TL. STREME: accurate and versatile sequence motif discovery. Bioinformatics.
1257 2021;37:2834–40.

98. Fernández R, Kallal RJ, Dimitrov D, Ballesteros JA, Arnedo MA, Giribet G, et al. Phylogenomics, Diversification Dynamics, and Comparative Transcriptomics across the Spider Tree of Life. Curr Biol. 2018;28:1489-1497.e5.

99. Jones P, Binns D, Chang H-Y, Fraser M, Li W, McAnulla C, et al. InterProScan 5: genome-scale protein function classification. Bioinformatics. 2014;30:1236–40.

100. Akiyama-Oda Y, Akaiwa T, Oda H. Supplementary Data for "Reconstruction of the Global Polarity of an Early Spider Embryo by Single-Cell and Single-Nucleus Transcriptome Analysis." figshare; 2022 [cited 2022 Jun 8]; Available from: https://doi.org/10.6084/m9.figshare.c.5963571.v1

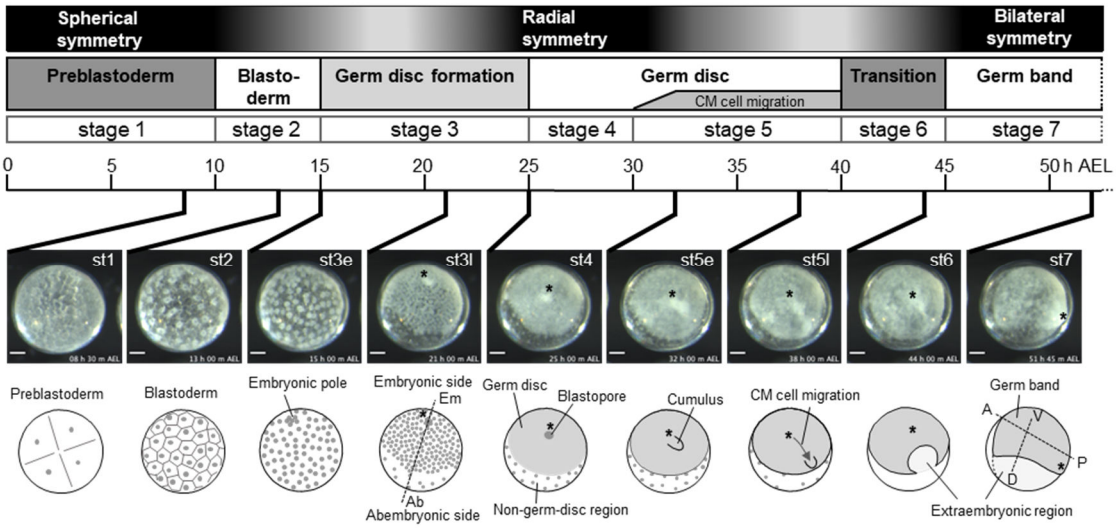

1268

1269 **Fig. 1. Early embryonic processes of *Parasteatoda tepidariorum*.** Selected time-lapse
1270 images of a live wild-type embryo (Additional file 1: Movie S1) are shown along with
1271 their timelines (time [h] after egg laying [AEL]), stages of development, and
1272 illustrations of morphological characteristics. The morphology of the developing *P.*
1273 *tepidariorum* embryo undergoes symmetry transitions as shown (top). An axis of radial
1274 symmetry (embryonic-abembryonic axis) and two axes of bilateral symmetry (anterior-
1275 posterior [A-P] and dorsal-ventral [D-V] axes) are indicated by broken lines. Asterisks
1276 mark cells around the embryonic pole, cells at the closed blastopore, and cells at the
1277 posterior pole, which are in the same lineage. Scale bars,100 μm.
1278

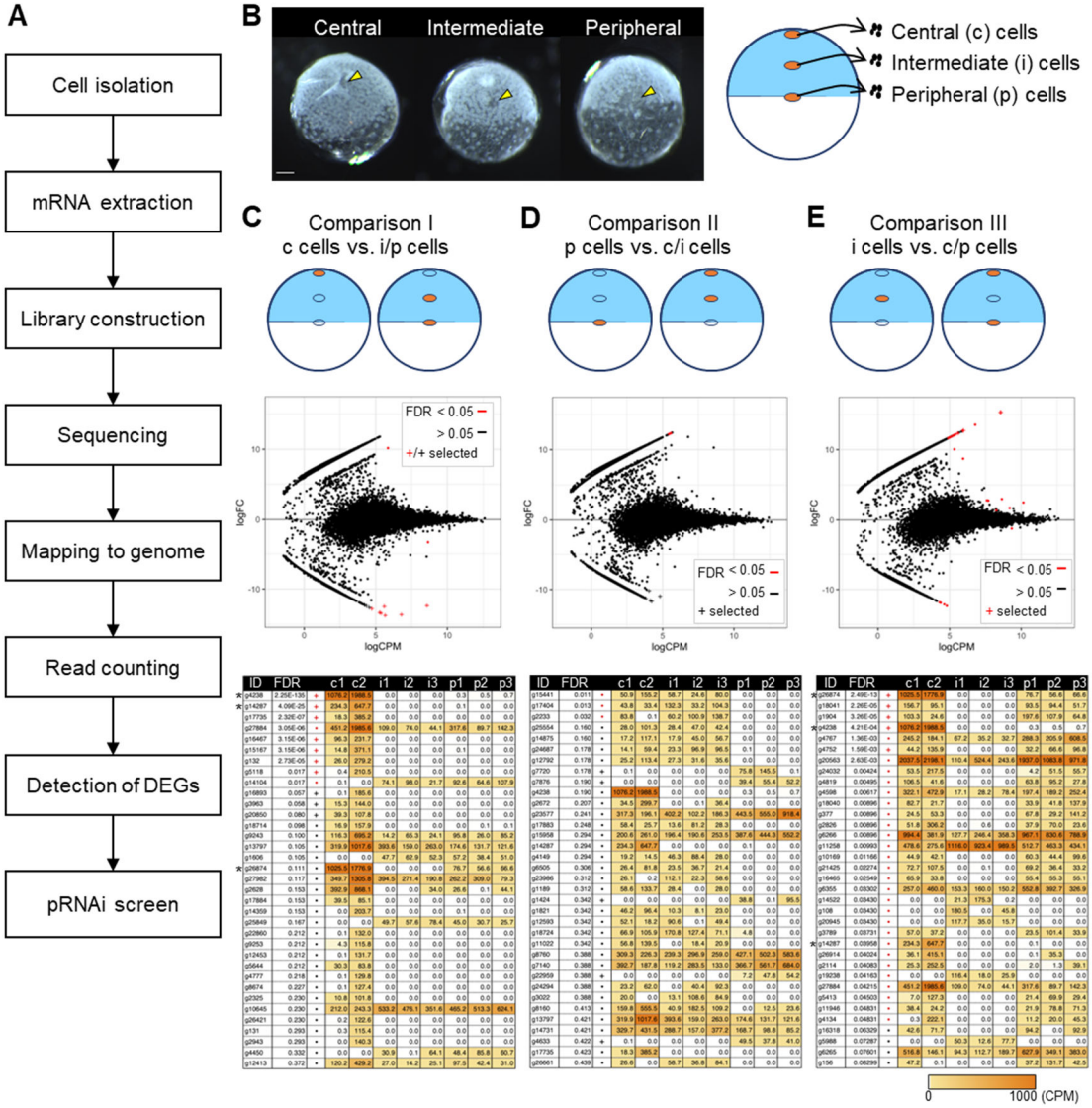

Fig. 2. Genome-wide identification of candidate genes with locally restricted expression in stage-3 embryo. (A) Outline of the experimental procedure. **(B)** Images showing live stage-3 embryos following isolation of cells from 3 different regions (yellow arrowheads; central [c], intermediate [i], and peripheral [p]) of the embryo, along with the schematic showing the isolated cells used for RNA-seq. Scale bar, 100 µm. **(C–E)** Three types of comparison using RNA-seq datasets from the c, i, and p cells (comparison I: c cells versus i/p cells [C]; comparison II: p cells versus c/i cells [D]; comparison III: i cells versus c/p cells [E]) detected candidates of differentially expressed genes (DEGs). Top: schematic showing the grouping of the datasets for comparison. Middle: MA-plot of $\log_2$ fold-change (FC) versus $\log_2$ average expression level (CPM; count per million) from 10,862 genes. Bottom: lists of DEG candidates

1291 with normalized expression levels (CPM) from biological replicates of the three sample
1292 types (c1, c2, i1, i2, i3, p1, p2, and p3), which are sorted by FDR values. Genes with
1293 FDR < 0.05 are highlighted in red, and candidates of DEGs that were selected for a
1294 pilot pRNAi screen are indicated by plus signs in the MA-plots and tables. Each table
1295 displays the top 35 genes; the full lists are presented in Additional file 2: Tables S1–
1296 S3. Note that genes marked by asterisks appear in multiple tables.
1297

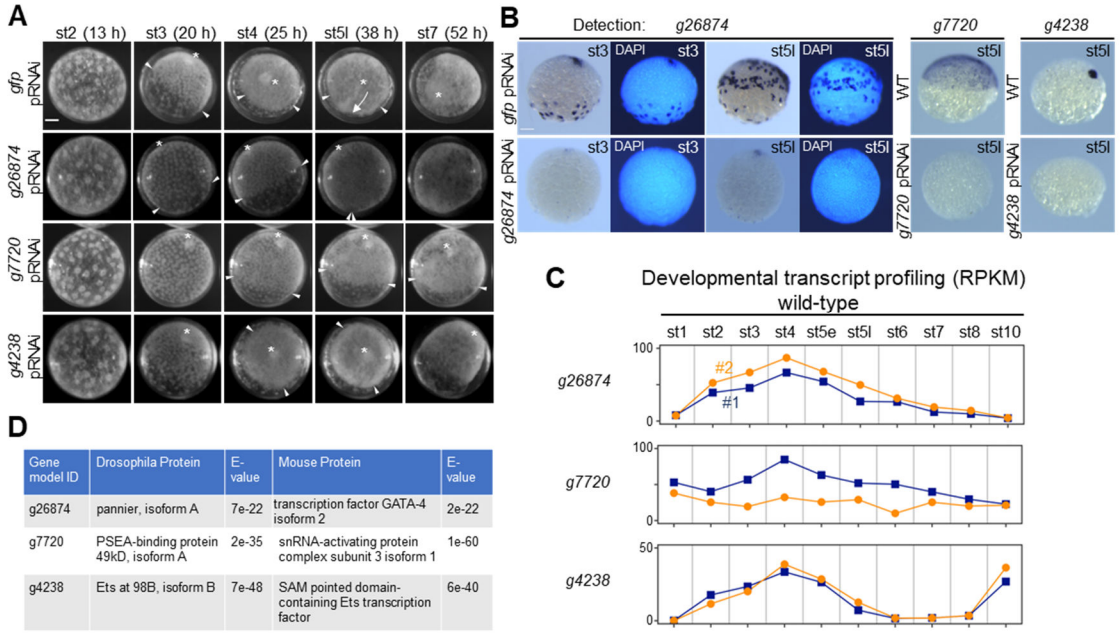

Gene model ID	Drosophila Protein	E-value	Mouse Protein	E-value
g26874	pannier, isoform A	7e-22	transcription factor GATA-4 isoform 2	2e-22
g7720	PSEA-binding protein 49kD, isoform A	2e-35	snRNA-activating protein complex subunit 3 isoform 1	1e-60
g4238	Ets at 98B, isoform B	7e-48	SAM pointed domain-containing Ets transcription factor	6e-40

Fig. 3. Identification of three genes in a pilot pRNAi screen of the DEG candidates. **(A)** Images showing the development of live *gfp* pRNAi, *g26874* pRNAi, *g7720* pRNAi, and *g4238* pRNAi embryos. These images are related to Movie S2 (Additional file 4). Stages of development and time (h) after egg laying (AEL) are shown. Asterisks indicate the embryonic pole, closed blastopore, and posterior pole. Arrowheads indicate the rim of the forming/formed germ disc, or corresponding sites in morphologically affected embryos. The arrow indicates CM cell migration, which did not occur in the *g26874* pRNAi, *g7720* pRNAi, and *g4238* RNAi embryos. **(B)** Effect of *g26874*, *g7720*, or *g4238* pRNAi on the expression of the corresponding target gene at stage 3 and/or late stage 5, as revealed by WISH. *gfp* pRNAi or wild-type (WT) embryos were stained as controls. Counterstains with DAPI were displayed for the comparison between *g26874* and *gfp* pRNAi embryos. **(C)** Graphs showing developmental profiling of the transcript levels (RPKM; reads per kilobase of transcript, per million mapped reads) for *g26874*, *g7720*, and *g4238* in wild-type embryos, based on public datasets [36]. Two biological replicates are individually shown. **(D)** Results of blast searches against *D. melanogaster* and mouse RefSeq protein databases using predicted amino acid sequences of *g26874*, *g7720*, and *g4238* as queries. The top-hit protein from each search is shown. Scale bars, 100 μm in A and B.

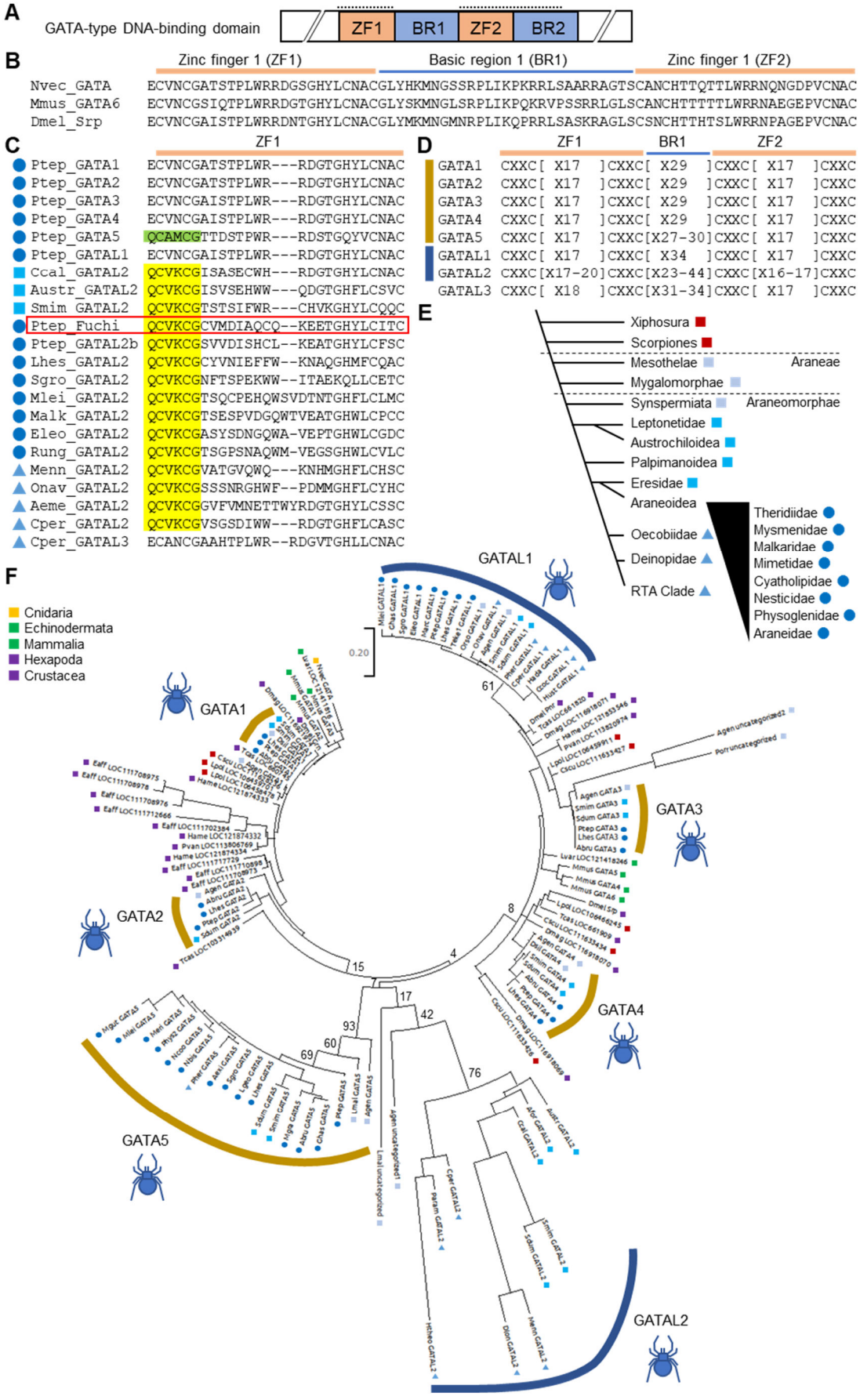

Fig. 4. Phylogenetic characterization of Fuchi and other spider GATA family proteins. (A) Schematic of GATA-type DNA-binding domain. This domain comprises two zinc finger motifs (ZF1 and ZF2) and two basic regions (BR1 and BR2). **(B)** Amino acid sequence alignment of the ZF1-BR1-ZF2 region (plus one adjacent residue on the N-terminal side) of three canonical GATA family members from cnidarian, mouse and *Drosophila* (Nvec_GATA, *Nematostella vectensis* GATA; Mmus_GATA6, *Mus musculus* GATA-6; Dmel_Srp, *Drosophila melanogaster* Serpent). **(C)** Amino acid sequence alignment of the ZF1 (plus one flanking residue on the N-terminal side) of various GATA family members from *P. tepidariorum* and other spider species. There are five canonical (Ptep_GATA1 to GATA5) and three noncanonical (Ptep_GATAL1, Fuchi, GATAL2b) GATA family members in *P. tepidariorum*. The GATAL2 group, including Fuchi, is characterized by the signature sequence highlighted in yellow, and the GATA5 group by the signature sequence highlighted in green. There are two types of GATAL2 proteins; the ZF1 of one type is aligned with that of the canonical GATA without gap but the ZF1 of the other type is not. **(D)** Classification of spider GATAs based on cysteine residue spacing patterns in the ZF1-BR1-ZF2 region. GATA5s in some spider species had a BR1 of slightly varied length. **(E)** Diagram showing phylogeny of spider taxa, based on a recent study [98]. **(F)** Maximum likelihood tree of canonical and non-canonical GATA family members from Araneae, non-Araneae chelicerates, non-chelicerate arthropods, non-arthropod bilaterians, and cnidarian, using 75 amino acid sites unambiguously alignable. GATAL2 proteins with imperfectly aligned ZF1, including Fuchi, were excluded from this analysis. Bootstrap values (100 replicates) are presented at selected nodes. Color geometric codes indicate taxonomic groups of the sequence source. Details of species names and sequences are available in Tables S7 and S8 (Additional file 7).

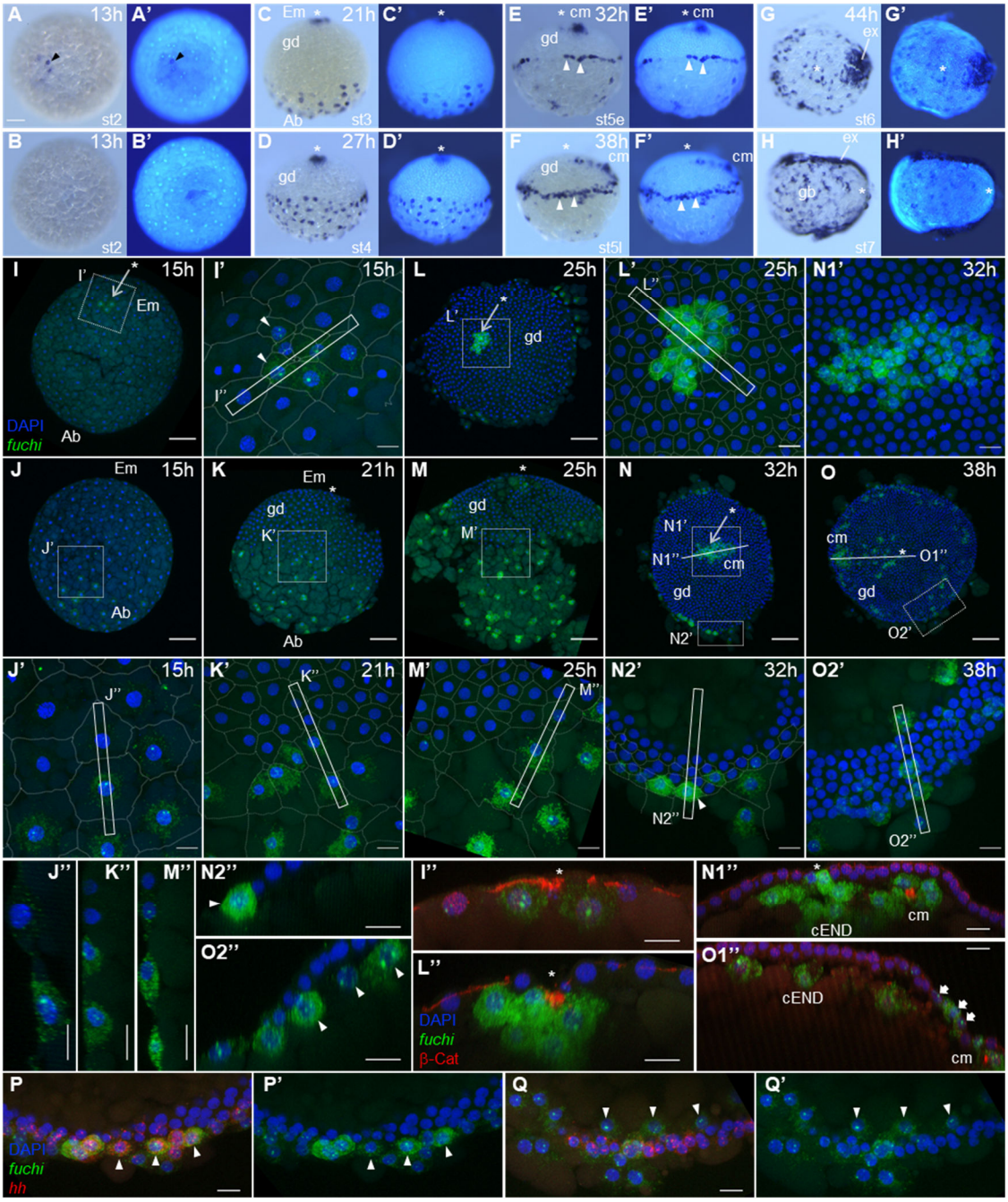

Fig. 5. Expression of *fuchi* transcript in specific cells on the embryonic and abembryonic sides of early embryos. (A–H) Chromogenic WISH of wild-type embryos at indicated stages using probes for *fuchi* transcript (left), counter-stained for DNA (right). **(A, B)** Opposite sides of the same embryo. Arrowhead indicates the signal. **(C–F)** Lateral view. The forming/formed germ disc (gd) is up. Arrowheads denote cells expressing *fuchi* at or near the germ-disc rim. **(G, H)** Forming germ band (gb) with expanding extraembryonic region (ex). Asterisks mark the embryonic pole, closed

blastopore, or posterior pole. **(I–O)** Reconstruction of confocal stacks showing wild-type embryos fluorescently stained for *fuchi* transcript (green) and DNA (blue) at 15 (I, J), 21 (K), 25 (L, M), 32 (N), and 38 (O) h AEL. Asterisks mark the embryonic pole or closed blastopore. I and J show the same embryo from different directions. **(I'–M', N1', N2', O2')** High magnification of the boxed areas in I–O. Cell-cell junctions visualized by staining for β-catenin are traced in I'–M', and N2'. **(I"–M", N2", O2")** Optical sections corresponding to the rectangular regions in I'–M', N2', and O2'. Arrowheads indicate *fuchi*-expressing cells that appear to be internalizing or internalized. **(N1", O1")** Optical sections corresponding to the lines in N and O. Signals for β-catenin are overlaid in red in I", L", N1", and O1". β-Catenin concentrations mark the cumulus (cm). Fat arrows indicate *fuchi* expression in the future extraembryonic region. **(P, P', Q, Q')** Simultaneous detection of *fuchi* (green) and *Pt-hh* (red) transcripts and DNA (blue) in cells at or near the germ-disc rim at early (P, P') and late (Q, Q') stage 5. Arrowheads indicate cells expressing both *fuchi* and *Pt-hh* before internalization and cells expressing only *fuchi* after internalization. Em, embryonic side; Ab, abembryonic side. Scale bars, 100 μm in A, I–O; 20 μm in other panels.

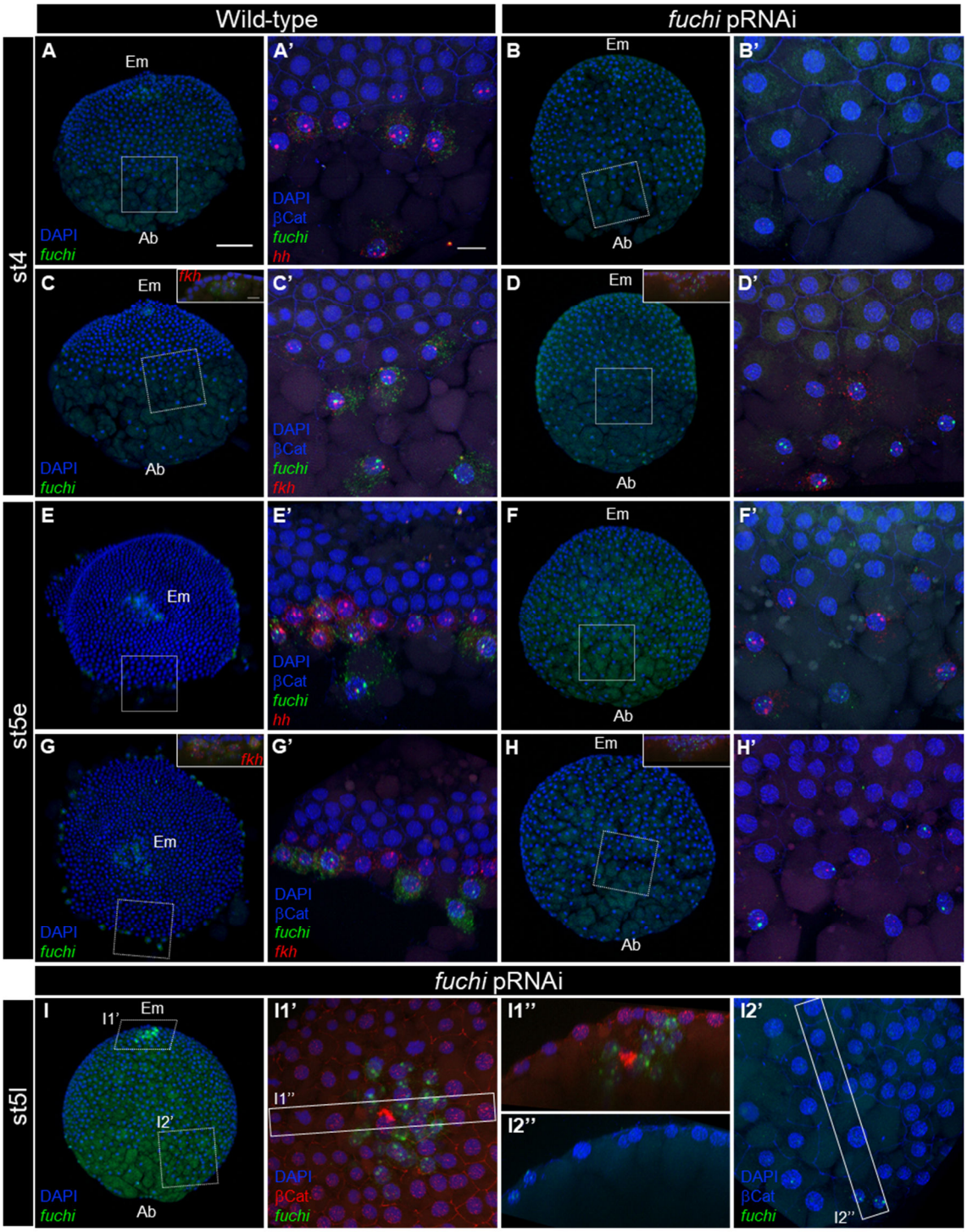

Fig. 6. Defects of *fuchi* pRNAi embryos in demarcating a forming germ disc. (A–H) Reconstructions of confocal stacks showing wild-type (A, C, E, G) and *fuchi* pRNAi (B, D, F, H) embryos stained for *fuchi* (green, A–H) and *Pt-hh* (red, A, B, E, F) or *Pt-fkh* (red, C, D, G, H) transcripts, DNA (blue, A–H), and β-catenin (blue, A'–H'; not shown in A-H) at stage 4 (A–D) and early stage 5 (E–H). In A–D, F, H, and I, the

1381 embryonic side (Em) is to top, with the abembryonic (Ab) to bottom. In E and G, the
1382 embryonic side is viewed from the top. Optical sections show the presence of specific
1383 cells expressing *fuchi* at the embryonic pole (insets, C, D, G, H). The boxed areas in
1384 A-H are magnified in A'-H', respectively. *fuchi* transcript was detectable even in cells
1385 on the abembryonic side of *fuchi* pRNAi embryos, although the signals were restricted
1386 to within the nuclei. Cells expressing *Pt-hh* and *Pt-fkh* transcripts at reduced levels
1387 were observed at regions corresponding to the the germ-disc rim and nearby
1388 abembryonic region in *fuchi* pRNAi embryos at early stage 5, but these cells did not
1389 serve as rim cells demarcating a forming germ disc. (I) Reconstructions of confocal
1390 stacks showing a *fuchi* pRNAi embryo stained for *fuchi* transcript (green, I, I1', I2'),
1391 DNA (blue, I, I1', I2'), and β-catenin (red, I1'; blue, I2') at late stage 5. (I1', I2') High
1392 magnification of the boxed areas in I as indicated. (I1", I2") Cross-sections of the
1393 rectangular regions in I1' and I2'. The cluster of CM cells were eventually internalized,
1394 but with few cells internalized in other regions. Note that the cells spread over the
1395 abembryonic side with epithelial integrity retained to a certain extent. Scale bars, 100
1396 μm in A; 20 μm in A', inset of C.
1397

1398

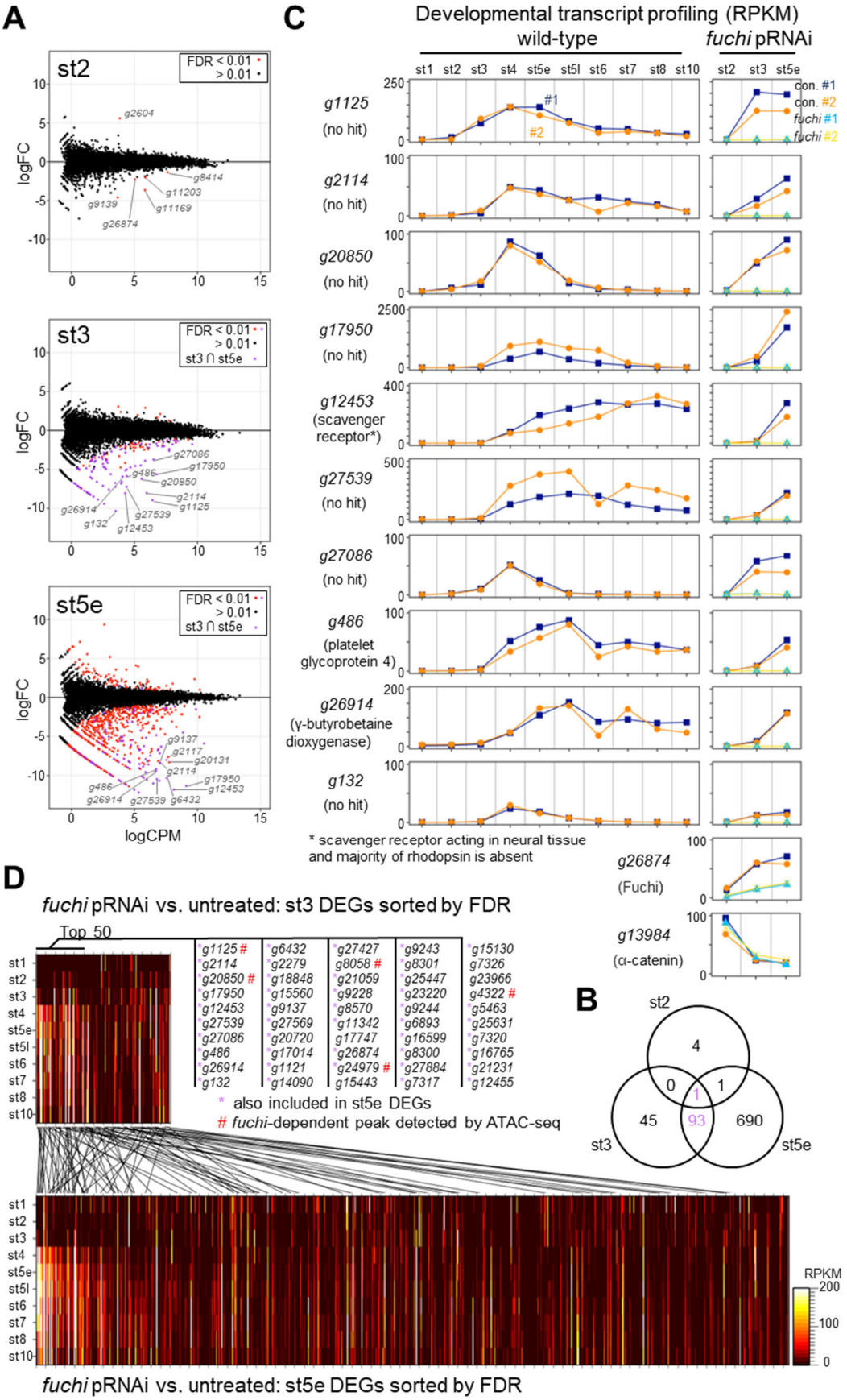

1399

Fig. 7. Genome-wide identification of genes whose expression levels are affected following *fuchi* knockdown. (A) MA-plots of $\log_2$ fold-change (FC) versus $\log_2$ average expression level (CPM) showing DEGs between *fuchi* pRNAi and control (untreated) embryos at stage 2 (st2), stage 3 (st3), and early stage 5 (st5e). Genes with FDR < 0.01 are highlighted in red or purple, with the purple genes included in both stage-3 and early stage-5 DEG lists. **(B)** Venn diagram showing the numbers of the DEGs from the three sample types and their overlaps. Note that *fuchi* (*g26874*) itself is included in all the DEG lists. **(C)** Graphs showing developmental profiling of the transcript levels for the top 10 DEGs from the stage-3 samples in wild-type embryos and the effects of *fuchi* pRNAi on the transcript levels. Top hit proteins that resulted from blastx searches against mouse and *Drosophila* RefSeq protein databases are shown, although with no hits obtained with seven of the ten genes (E-value < 1e-5). Data on *fuchi* (*g26874*) and α-catenin (*g13984*) validated the experiments. **(D)** Heat maps showing developmental profiling of the transcript levels for all the DEGs from the stage-3 (upper) and early stage-5 (lower) samples in wild-type embryos (sorted by FDR values). The top 50 DEGs from stage-3 are listed, where the genes included in stage-5 DEGs are indicated by purple asterisks. Genomic regions differentially accessible between wild-type and *fuchi* pRNAi embryos at stage 3 were found to be located within or close to some of the DEGs marked by "#"(related to Fig. 8 and Additional file 10: Table S13).

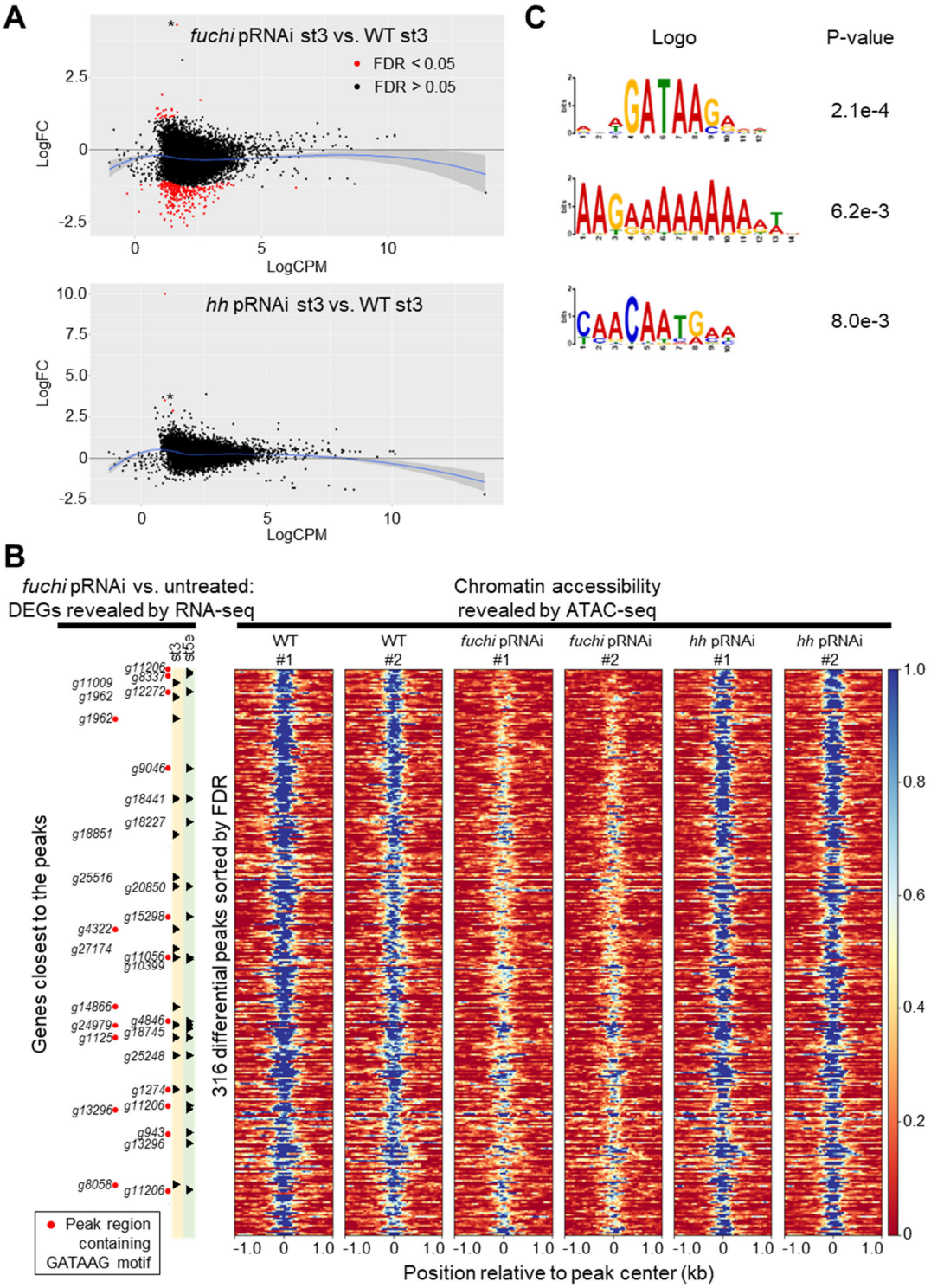

Fig. 8. Effect of *fuchi* knockdown on chromatin accessibility in specific genomic regions in stage-3 embryos. (A) Distributions of differentially accessible genomic regions identified by comparisons between ATAC-seq datasets from *fuchi* (upper) or *Pt-hh* (lower) pRNAi and wild-type embryos. MA-plots represent $\log_2$ fold-change

(FC) versus $\log_2$ average ATAC signal abundance (CPM). Two biological replicates were obtained from each sample type and analyzed. Significant differentially accessible regions (FDR < 0.05) are highlighted in red. Blue lines are loess fits to each distribution with 95% confidence intervals shaded in gray. Asterisks indicate positive peaks at the same genomic region. Detection of this region might not be specific to *fuchi* activity. **(B)** Heat maps showing chromatin accessibilities in the 316 genomic regions identified as *fuchi*-dependent (sorted by FDR values). Data from the biological replicates are individually shown. Some of the identified regions are located close to or within the loci of DEGs identified by the RNA-seq analyses, as shown on the left side. **(C)** Motif sequences enriched in the *fuchi*-dependent peaks, as revealed by a motif discovery tool STREME [97]. Peak regions containing detected motif sequences, RNWGATAAGAVW, are indicated in B (red dots).

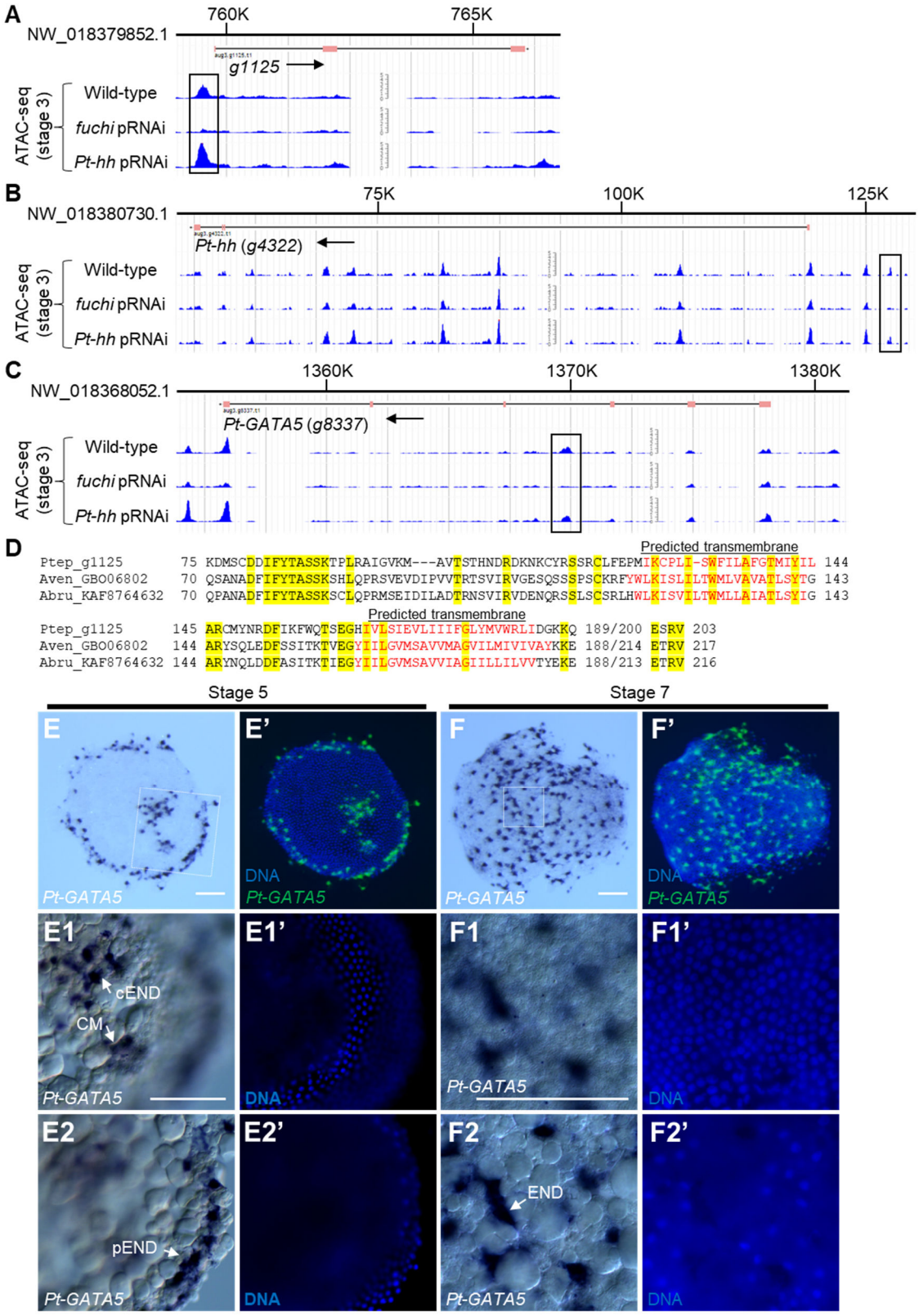

Fig. 9. Three notable examples of genes revealed by combined analyses of the RNA-seq and ATAC-seq datasets. (A–C) Normalized ATAC-seq signal of stage-3 wild-type, *fuchi* pRNAi, and *Pt-hh* pRNAi embryo at the *g1125* (A), *Pt-hh* (*g4322*) (B), and *Pt-GATA5* (*g8337*) (C) loci. Line with ticks at the top represents the scaffold sequence, below which annotated exons (pink boxes) and introns (black lines) are shown. *fuchi*-dependent peak regions are indicated by open rectangles. Arrows indicate the orientation of the gene. **(D)** Amino acid sequence alignment of the *g1125* protein and its homologs detected in the genomes of two other spider species *Araneus ventricosus* (GBO06802.1) and *Argiope bruennichi* (KAF8764632.1). Residues identical across all proteins are presented with a yellow background. Residues shown in red indicate regions predicted as transmembrane domains by InterProScan version 5.53-87.0 [99]. **(E, F)** Detection of *Pt-GATA5* transcript and DNA (E', F') in stage-5 (E) and stage-7 (F) embryos using chromogenic WISH. **(E1, E2, F1, F2)** High magnification of the boxed areas in E and F, along with counter staining for DNA (E1', E2', F1', F2'). The focal plane is at two different depths; the plane shown in E2 and F2 is deeper than that in E1 and F1, respectively. Signals are observed in cEND, CM, and pEND cells, which are located below the germ-disc epithelial layer, and in evenly distributed endoderm (END) cells, which are located below the germ-band epithelial layer. Scale bars, 100 μm.